

Master Thesis

# Implementation of a handheld UWB antenna for automotive applications

**Paul Unterhuber**

**Institute of Microwave and Photonic Engineering,**

Graz University of Technology



**Maxim Integrated**



Supervisor: Ao.-Prof. Dipl.-Ing. Dr.techn. Erich Leitgeb

Dott.-Ing. Ivan Russo

Dipl.-Ing. Dr.techn. Thomas Gigl

Graz, Mai 2013



## **Eidesstattliche Erklärung**

Ich erkläre hiermit, dass ich die vorliegende Arbeit selbstständig verfasst, keine anderen als die angegebenen Quellen und Hilfsmittel benutzt und wörtlich und inhaltlich entnommene Stellen als solche gekennzeichnet habe.

Graz, am 22. Mai 2013

---

(Paul Unterhuber)

## **Statutory declaration**

I declare that I have authored this thesis independently, that I have not used other than the declared sources and resources and that I have explicitly marked all material which has been quoted either literally or by content from the used sources.

Graz, Mai 22<sup>nd</sup>, 2013

---

(Paul Unterhuber)

## **Abstract**

In 2002 the Federal Communications Commission (FCC) published the first specifications for Ultra Wide Band (UWB) data communications. Since then, UWB has been developed into a well-used and practical wireless communication standard, offering a high data transmission rate with low power consumption over a wide bandwidth.

The aim of this thesis is to investigate the handset part of a broadband system for automotive applications. In particular, an antenna with an operation frequency of 4 GHz and a relative bandwidth of 25% should be developed. From these specifications it is evident that the main objective is focalized on the miniaturization of the antenna structure to fit in the given handset, in this case a car key with 5 x 3 cm size. This key is used for locking and starting the car with a keyless system. Therefore the key has to be able to connect with the car in any possible orientation of the key. To simplify the key components, the antenna should be linearly polarized.

This thesis is divided in three parts. The first part shows a short overview of antenna basics and the used simulation program. In the second part, the investigation of already known UWB antenna structures and broadband antennas, regarding the key system are documented. After a detailed literature research and taking into account all specifications, the first approach was done with dipole antennas. The last part shows the results for suitable antennas. Furthermore simulations with two very small antennas placed in the key and the whole key in a human environment are shown. Also the realized prototype, the antenna systems in the key and the measurement and test results are shown.

## Kurzfassung

Im Jahr 2002 wurden die ersten Spezifikationen für Ultra Wide Band (UWB) Datenkommunikation von der Federal Communications Commission (FCC) veröffentlicht. Seither hat sich UWB zu einem weit verbreiteten Funkstandard entwickelt. Dieser Standard bietet eine Datenübertragung mit hohen Übertragungsraten in Kombination mit niedrigen Energieaufkommen.

Das Ziel dieser Diplomarbeit ist die Untersuchung und der Aufbau eines Handgerätes (Schlüssel) für ein Breitbandkommunikationssystem. Dieses System soll für Fahrzeuganwendungen eingesetzt werden. Die Arbeit umfasst die Entwicklung und das Design einer Antenne für eine operative Frequenz von 4 GHz und einer relativen Bandbreite von 25%. Aufgrund des geringen Platzangebotes im Handgerät von ca. 5 x 3 cm liegt das Hauptaugenmerk auf speziellen Techniken zur Verkleinerung der Antennengröße. Der Schlüssel soll zum schlüssellosen Sperren und Entsperren sowie zum Starten des Fahrzeugs verwendet werden. Dafür muss eine Kommunikation zwischen Schlüssel und Auto in jeglicher Lage des Schlüssels zum Auto möglich sein. Um die Antenne zu vereinfachen wird eine linear polarisierte Antenne verwendet.

Die Arbeit ist unterteilt in drei Bereiche. Zuerst wird ein kurzer Überblick über Antennentheorie- und Grundlagen gegeben. Der zweite Teil zeigt die Ergebnisse der Literatur Recherche von bereits vorhandenen Realisierungsmöglichkeiten. Aus dieser Untersuchung ergaben sich Dipole als bestmögliche Realisierungsmöglichkeit. Im letzten Teil werden die Simulationen und Ergebnisse der Messungen dokumentiert und beschrieben.

## Acknowledgments

For the academical supervision I would like to thank *Prof. Dr. Erich Leitgeb* and *Dr. Ivan Russo*, who guided me through the theoretical and practical challenges of this project, and helped with word and deed if needed. Furthermore, I would like to express thanks to the Institute of Microwave and Photonic Engineering for the provision of technical equipment.

Special thanks are due to “Maxim Integrated”, represented by *Dr. Gerhard Schultes* and my supervisor *Dr. Thomas Gigl* who initialized and funded this thesis.

*Vielen Dank,*

*Merci!*

# Table of Content

1	INTRODUCTION	1
1.1	Motivation	1
1.2	Requirements	1
2	ANTENNA BASICS	3
2.1	Bandwidth	3
2.2	Center frequency	3
2.3	Wavelength	4
2.4	Antenna length	4
2.5	Input Impedance	4
2.6	Directivity	5
2.7	Gain	5
2.8	Polarization	6
2.9	Cross polarization and axial ratio	6
2.10	Group delay	6
3	CST STUDIO SUITE®	7
3.1	Simulation settings	7
3.2	Simulation results	7
3.2.1	Reflection and coupling coefficient	7
3.2.2	Line characteristic impedance	8
3.2.3	Radiation pattern	8
3.2.4	Gain	8
3.2.5	Cross-polarization	8
3.2.6	Group delay	9
3.3	Charts and coordinate systems	9
3.4	External influence factors	10
4	CONCEPT STUDIES AND EVALUATION	11
4.1	Dipole antennas	11
4.1.1	Radiator shapes	12

4.1.2 Summary of printed dipole antennas	15
4.2 Monopole antennas	16
4.2.1 Radiator shapes	16
4.2.2 Feed and ground plane	17
4.2.3 Summary of printed monopole antennas	19
4.3 Planar inverted antennas	21
4.3.1 Inverted-L antenna (ILA)	21
4.3.2 Inverted-F antenna (IFA)	21
4.3.3 Summary of PIFAs	23
4.4 Conclusions of the literature research	24
5 IMPLEMENTATION OF MINIATURIZED UWB DIPOLE ANTENNAS	25
5.1 Stages of development	25
5.1.1 Basic structure	25
5.1.2 Miniaturization with permittivity $\epsilon_r$	26
5.1.3 Double radiators	26
5.1.4 Input impedance	27
5.2 Simulations	28
5.2.1 Parameters	28
5.2.2 Reflection coefficient $S_{11}$	30
5.2.3 Coupling coefficient $S_{12}$	33
5.2.4 Antenna pattern	35
5.2.5 Antenna gain	40
5.2.6 Group delay	41
5.2.7 Cross-polarization ratio	42
5.3 Prototype manufacturing	43
5.4 Measurements	44
5.4.1 Measurement equipment	44
5.4.2 Connection techniques	45
5.4.3 Reflection coefficients $S_{11}$ and $S_{22}$	46
5.4.4 Coupling coefficients $S_{12}$ and $S_{21}$	47
5.4.5 Antenna pattern	48
5.4.6 Antenna gain	51
5.4.7 Group delay	52

6	PLANAR INVERTED-F ANTENNAS	54
6.1	Stages of development	54
6.1.1	Radiator	54
6.1.2	Substrate	54
6.1.3	Feeding structure	55
6.1.4	Ground plane	55
6.2	Simulations	56
6.2.1	Parameters	56
6.2.2	Reflection coefficient $S_{11}$	58
6.2.3	Antenna pattern	61
7	CONCLUSIONS	64
7.1	Results	64
7.2	Future Work	65
	BIBLIOGRAPHY	66

# List of Figures

Figure 1: Handset board	2
Figure 2: Spherical and Cartesian Coordinate systems	9
Figure 3: Dipole antenna [3]	12
Figure 4: Bowtie dipole antenna [2]	13
Figure 5: Diamond dipole antenna [2]	13
Figure 6: Rounded feed side diamond antenna	13
Figure 7: Elliptical dipole antenna [2]	14
Figure 8: Rectangular dipole antenna	14
Figure 9: Monopole antenna [3]	16
Figure 10: Bowtie monopole antenna	16
Figure 11: Triangular monopole antenna [2]	17
Figure 12: Elliptical monopole antenna	17
Figure 13: Rectangular monopole antenna [2]	17
Figure 14: Diamond monopole antenna	17
Figure 15: MS feed [15]	18
Figure 16: CPW feed [15]	19
Figure 17: Inverted-L antenna [23]	21
Figure 18: Inverted-F antenna [23]	21
Figure 19: Planar inverted-F antenna [24]	22
Figure 20: Elliptical dipole basic shape	26
Figure 21: Double elliptical dipole for 200 $\Omega$	27
Figure 22: Double dipole parameters	28
Figure 23: $S_{11}$ comparison for PCB parts	30
Figure 24: $S_{11}$ comparison for PCB surrounding	30
Figure 25: Key in hand simulation design	31
Figure 26: $S_{11}$ comparison for different radiator rotations (legend see Table 5)	32

Figure 27: $S_{12}$ comparison for PCB parts	33
Figure 28: $S_{12}$ comparison for PCB surrounding	33
Figure 29: $S_{12}$ comparison for different radiator rotations (legend see Table 5)	34
Figure 30: Far-field plot with D12 for different frequencies:	35
Figure 31: Far-field plot with D12 and battery for different frequencies:	36
Figure 32: Far-field plot of the double antenna with PCB disturbances:	37
Figure 33: Far-field plot for PCB surrounding:	38
Figure 34: Farfield plot for different radiator rotations (for the legend see Table 5)	39
Figure 35: Antenna gain with or without battery	41
Figure 36: Group delay with or without Battery	41
Figure 37: Cross-polarization in different directions	42
Figure 38: Gerber-file for PCB production	43
Figure 39: Rohde&Schwarz Vector Network Analyzer	44
Figure 40: Balun [30]	45
Figure 41: S-parameter measurement	46
Figure 42: $S_{11}$ and $S_{22}$ measured and simulated	46
Figure 43: $S_{12}$ and $S_{21}$ measured and simulated	47
Figure 44: Measurement chamber	48
Figure 45: Far-field plot for different frequencies:	49
Figure 46: Far-field plot comparison of measured and simulated at 4 GHz:	50
Figure 47: Connected antenna in the chamber	51
Figure 48: Antenna gain	52
Figure 49: Measurement setup group delay	52
Figure 50: Group delay measured and simulated	53
Figure 51: PIFA design	55
Figure 52: PIFA parameters	56
Figure 53: $S_{11}$ comparison for flat feed with different substrate	58
Figure 54: $S_{11}$ comparison for round feed with different substrate	58

Figure 55: $S_{11}$ comparison for round feed with different $d$	59
Figure 56: $S_{11}$ comparison for round feed with different $shift\_feed$	60
Figure 57: $S_{11}$ comparison for round feed with different $gnd\_x$	60
Figure 58: $S_{11}$ comparison for round feed with different $gnd\_y$	61
Figure 59: Far-field plot with PIFA for different frequencies:	62

## List of Tables

Table 1: Comparison of dipole antennas	15
Table 2: Comparison of monopole antennas	20
Table 3: Comparison of planar inverted-F antennas	23
Table 4: Dipole antenna parameters	29
Table 5: Comparison of different board sizes and radiator angles	32
Table 6: PIFA parameters	57
Table 7: Final results	64

## List of Abbreviations and Symbols

BW	bandwidth
CPW	co planar waveguide
CST	Computer Simulation Technology
DUT	Device under test
FCC	Federal Communications Commission
IC	integrated circuit
IFA	inverted-F antenna
ILA	inverted-L antenna
LF	low frequency
MS	micro strip
PCB	printed circuit board
PIFA	planar inverted-F antenna
RF	radio frequency
UWB	ultra wide band
VSWR	voltage standing wave ratio
$\alpha$	opening angle
$c$	speed of light = 299,792,458 m/s $\approx 3 \cdot 10^8$ m/s
$D_0$	maximum directivity
$e_0$	total efficiency (also known as $\eta$ )
$e_{cd}$	antenna radiation efficiency
$e_r$	reflection (mismatch) efficiency = $(1 -  \Gamma ^2)$
$\epsilon_r$	permittivity
$f_c$	center frequency
$f_H$	high frequency

$f_L$	low frequency
$G, G_0$	gain
$G_{0abs}$	gain absolute
$\lambda$	wavelength
$L$	length
$L_D$	dipole length
$L_M$	monopole length
$\phi$	time phase shift
$P_{rad}$	total radiated power
$r, r_1, r_2$	radii
$R_A$	antenna resistance
$R_r$	radiation resistance of the antenna
$R_L$	loss resistance of the antenna
$S_{11}$	reflection coefficient first antenna
$S_{12}$	isolation coefficient first to second antenna
$S_{21}$	isolation coefficient second to first antenna
$S_{22}$	reflection coefficient second antenna
$\tau_g$	group delay
$\delta$	loss tangent
$U_{max}$	radiation intensity
$W$	width
$X_A$	antenna reactance
$Z_A$	antenna impedance

# 1 Introduction

This thesis documents the development of two different designs for an antenna in an ultra-wide-band keyless entry communication system for an automotive application. The focus is on the handheld antenna.

## 1.1 Motivation

In 2002 the Federal Communications Commission (FCC) published the first specifications [1] for UWB data communications. Since then, UWB has been developed into a well-used and practical wireless communication standard, offering a high data transmission rate with low power consumption over a wide bandwidth [2].

The goal of this thesis is to investigate the handset part of a broadband system for automotive applications. In particular, an antenna should be developed with the requirements mentioned in the following part 1.2. Due to these specifications it is evident that the main objective is focalized on the miniaturization of the antenna structure to fit in the given handset, in this case a car key. This key is used for locking and starting the car with a keyless system.

## 1.2 Requirements

Considering the specifications of the car key, the following RF-requirements are given for the antenna in the handset:

- Broadband antenna
- $f_c = 4$  GHz
- $B > 500$  MHz
- $G \approx 0$  dB
- Quasi-omnidirectional pattern
- Linearly polarized

In addition to the RF-requirements, also the dimensions of the antenna have to be considered. Due to the limited space in the handset next to a battery and other RF-circuitry, the total dimension of the antenna system is the main challenge. The two given dimensions for the key PCBs are around  $4 \times 3 \text{ cm}^2$  and  $5 \times 3 \text{ cm}^2$ . Figure 1 shows the typical print board of the car key. The included parts are listed below:

- Battery  $\varnothing 2 \text{ cm}$
- Main IC  $0.6 \times 0.6 \text{ cm}^2$  (black IC in the middle of Figure 1)
- LF-tool  $1.1 \times 1.1 \text{ cm}^2$  (white IC, left side of Figure 1)

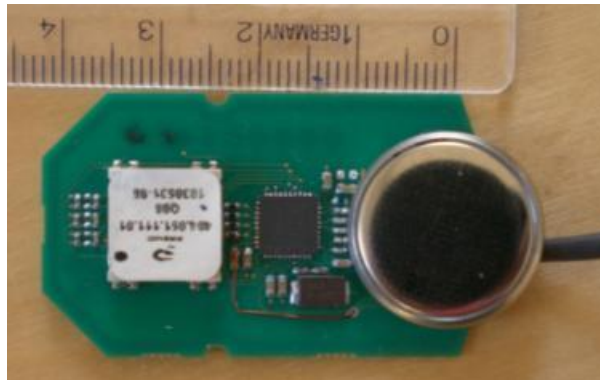


Figure 1: Handset board

These existing circuits will be also implemented in a new key but the design and the exact place may change for the next PCB design considering the broadband antenna and their subsystem.

## 2 Antenna basics

This chapter gives a short overview of the commonly used physical and mathematical basics for antennas. It is a summary of mathematical derivations and background information from “Antenna Theory, Analysis and Design” [3]. The equations the results of the specifications are shown in the following paragraphs. The parameters explained in this section are calculated as example and the requirements used for the actual design in this thesis are taken as numerical inputs.

### 2.1 Bandwidth

The bandwidth of an antenna is defined as “the range of frequencies within which the performance of the antenna, with respect to some characteristic, conforms to a specified standard”. The bandwidth is the frequency range around the center frequency  $f_C$ . Within this range, a specific antenna parameter (matching, axial ratio, cross-pol ratio, gain, etc.) fulfills some pre-defined requirements. The bandwidth can be described as absolute or relative bandwidth or as ratio between upper to lower frequencies [3] (not used here).

- Absolute bandwidth

$$BW = f_H - f_L \quad (2.1)$$

$$BW = 4.5 - 3.5 \text{ GHz} = 1 \text{ GHz}$$

- Relative bandwidth

$$BW = \frac{f_H - f_L}{f_C} \quad (2.2)$$

$$BW = 25 \%$$

### 2.2 Center frequency

As already mentioned before and as one the name suggests, the center frequency  $f_C$  is the center of the used frequency band, limited by the high and low frequencies  $f_H$  and  $f_L$ .

$$f_C = \frac{1}{2}(f_H + f_L) \quad (2.3)$$

$$f_C = 4 \text{ GHz}$$

## 2.3 Wavelength

The wavelength is a very important design parameter for antennas. It is indirectly proportional to the frequency and directly proportional to the geometrical dimension of an antenna.

$$\lambda = \frac{c}{f_c} \quad (2.4)$$

For example, the free space wavelength at 4 GHz in the case of vacuum is:

$$\lambda = \frac{3 \cdot 10^8 \text{ m/s}}{4 \cdot 10^9 \text{ 1/s}} = 74.95 \text{ mm}$$

## 2.4 Antenna length

For most common antennas like dipoles or monopoles, the antenna length is the determining coefficient for its current distribution and thus for its radiation properties. For conventional antenna types, the length usually varies between a quarter to a half a wavelength. With different techniques (see Chapter 4) the antenna length can be further decreased.

- Dipole length

$$L_D = \frac{\lambda}{2} \quad (2.5)$$

$$L_D = 37.47 \text{ mm}$$

- Monopole length

$$L_M = \frac{\lambda}{4} \quad (2.6)$$

$$L_M = 18.74 \text{ mm}$$

## 2.5 Input Impedance

The input impedance  $Z_A$  is defined as the impedance presented by an antenna at its terminals [3].

$$Z_A = R_A + jX_A \quad (2.7)$$

$$R_A = R_r + R_L \quad (2.8)$$

Caused by the fact that an antenna is always plugged to a generator or IC with a cable, the antenna impedance has to be considered. The antenna should match its subsystems to provide the minimum reflection losses due to impedance discontinuity. Being  $Z_g = R_g + jX_g$  the impedance seen at the antenna terminals towards the source, the condition that provides the maximum power transfer at the antenna itself is.

$$Z_A = Z_g^* \quad (2.9)$$

## 2.6 Directivity

The directivity  $D$  of a non-isotropic source is equal to the ratio of its radiation intensity in a given direction over that of an isotropic source. It defines the ability of an antenna to direct (concentrate) the radiated power in a specific direction and with a given angular aperture. An antenna with directivity equal to one defines an ideal isotropic radiator, which radiates the same amount of power to each direction of the surrounding environment. In general there are preferred directions of radiation, which defines the antenna lobes (global and local maxima).

$$D_0 = 4\pi \frac{U_{\max}}{P_{\text{rad}}} \quad (2.10)$$

The maximum directivity  $D_0$  refers to the directivity towards the direction of maximum radiation intensity [3].

$$D_0 = D_{\max} = 4\pi \frac{U_{\max}}{P_{\text{rad}}} \quad (2.11)$$

## 2.7 Gain

The gain  $G$  of an antenna is directly connected to its directivity  $D$  under and its radiation efficiency  $e_0 = e_r e_{cd}$  which is used to consider all the losses like input losses ( $e_r$  reflections because of mismatch) and within the structure ( $e_{cd}$  conduction and dielectric). The maximum gain includes only internal losses through  $e_{cd}$  while the maximum absolute or realized gain includes all losses ( $e_0$ ).

$$G_0 = e_{cd} * D_0 \quad (2.12)$$

$$G_{0\text{abs}} = e_0 * D_0 \quad (2.13)$$

## 2.8 Polarization

The polarization of an antenna is the capability of an antenna to produce a wave, which oscillates along a specific path during its propagation along the direction of radiation. It describes the time varying direction and relative magnitude of an electric field vector. There are three polarization types:

- Linear polarization
- Circular polarization
- Elliptical polarization

For this application, mounted in a handset with dimensions as small as possible, only a linear polarized antenna is possible. A linear polarization can be generated if only one transversal component of the far field wave is present (longitudinal components are identically null in far field because a local plane wave is propagating) or if the following phase relation between the two orthogonal transversal components is fulfilled:

$$\Delta\phi = \phi_y - \phi_x = n\pi \quad n = 0,1,2,3, \dots \quad (2.14)$$

## 2.9 Cross polarization and axial ratio

The cross polarization ratio is the ratio between the magnitude of the main polarization and the magnitude of the correspondent orthogonal polarization. This figure of merit describes the amount of undesired polarization component for linearly polarized antennas, hence the spurious radiation.

The axial ratio is the ratio between the magnitudes of the  $\theta$  and  $\phi$ -plane. It describes the polarization ratio for circularly and elliptically polarized antennas. A value of one identifies a perfectly circularly polarized antenna, provides that the phase difference between the x- and y-components is  $90^\circ$ .

## 2.10 Group delay

The frequency dependence of the time delay is characterized by the group delay of an antenna [4]. In point of interest is the relative group delay for a certain frequency range. This antenna parameter should be low and constant or weak oscillating.

## 3 CST Studio Suite<sup>®</sup>

In this thesis CST Studio Suite<sup>®</sup> [5] is used for all simulations. CST Studio Suite is a common used simulation program and its packet Microwave Studio is specialized on 3D EM simulations. The main part of these simulations is done with the CST Microwave Studio and simulated with the Time Domain Solver . This solver is based on the Finite Integral Technique, which consists in a discretization of the simulation domain in cubic cells defined as meshes. The integral equations are then solved with proper boundaries to determine electric and magnetic fields at the edges and faces of such cells. The overall solution is obtained by the combination of each discrete solution. The simulation domain is enclosed within a PML material (Perfect Matching Layer) that avoids undesired numerical reflections at the borders of the simulation domain. A further near-to-far-field transformation allows the calculation of the radiated far fields. The method is performed after the excitation of the structure under test with an input signal (normally a pulse).

### 3.1 Simulation settings

The settings for the simulations in CST Microwave studio are mentioned below.

- Frequency 2 – 6 GHz
- Mesh cells:
  - Lines per wavelength: 20
  - Lower mesh limit: 20
  - Mesh line ratio limit: 20
- Accuracy -30 dB or -80 dB
- Signal: Gaussian impulse
- Farfield monitor at 4 GHz

### 3.2 Simulation results

For the simulations the following results are of interests.

#### 3.2.1 Reflection and coupling coefficient

The reflection coefficient  $S_{11}$  represents how much power is reflected and radiated by the antenna. The desired  $S_{11}$  for the used bandwidth should be smaller than -10 dB. In these

simulations,  $S_{11}$  represents the reflection coefficient of port 1 and  $S_{22}$  the reflection coefficient of port 2.

In case of an antenna array the coupling coefficient  $S_{12}$  describes the transmitted power from one antenna to another. For this application,  $S_{12}$  depicts the power transferred from port 2 to port 1 and  $S_{21}$  represents this process the other way round. The inverse of the coupling coefficients provide the isolation coefficient between the ports.

### 3.2.2 Line characteristic impedance

To get a good match with the sub-circuits the feeding structure must be designed for the required line impedance. The line characteristic impedance should be  $50 \Omega$  (over GND) for measurements and  $200 \Omega$  (differential) for the application itself.

### 3.2.3 Radiation pattern

The radiation pattern can be plotted as a planar 2D or a 3D plot. Within the settings the directivity, the gain after the IEEE definition, the realized gain or other parameters can be chosen. For one frequency the field monitor analyzes the farfield properties of the antenna in any direction. To address the purposes of this thesis, the radiation pattern has been valued at the frequencies 3.5 GHz, 3.75 GHz, 4 GHz, 4.25 GHz and 4.5 GHz.

### 3.2.4 Gain

The gain can be plotted in two ways, for every direction or for every frequency. After having analyzed the radiation pattern simulations, the gain can be shown for any direction. The post-processing function "broadband monitor" calculates the realized gain for the whole spectrum with the limitations of one direction. The result is a graph showing the gain over the used frequency band in a 2D plot.

### 3.2.5 Cross-polarization

In case of the double dipole antenna, the cross polarization has to be simulated like a dual polarized antenna. For an omnidirectional antenna the cross-polarization should be approximately equal for any direction. In order to evaluate the cross-polarization ratio, linear E-field probes are placed in all directions around the antenna pair. To cover every side ( $\pm x$ -,  $y$ -,  $z$ -direction), 6x2 orthogonal probes are placed at farfield distance ( $\approx 200$  mm) around the

PCB. For each direction 2 orthogonal vectors (ports) are simulated. The ratio of each pair delivers the cross-polarization ratio for each correspondent direction.

### 3.2.6 Group delay

The group delay was simulated by using 2 equal prints in a distance of 30 cm (far field conditions). Because of a technical limitation in CST only two simulation ports can be used for this procedure. Therefore the other two antennas are matched with lumped elements.

## 3.3 Charts and coordinate systems

The simulation- and measurement results are shown in 2D or 3D plots.

The 2D plots show the measured amplitude over the frequency (in GHz) or, in case of the group delay over the time (in ns). The results are shown in rectangular windows and the far-field plots in polar charts. The polar plots are sectional images of the pattern for different  $\phi$  ( $0^\circ$ - $90^\circ$ ) and  $\theta$  ( $0^\circ$ ,  $90^\circ$ ) angles.

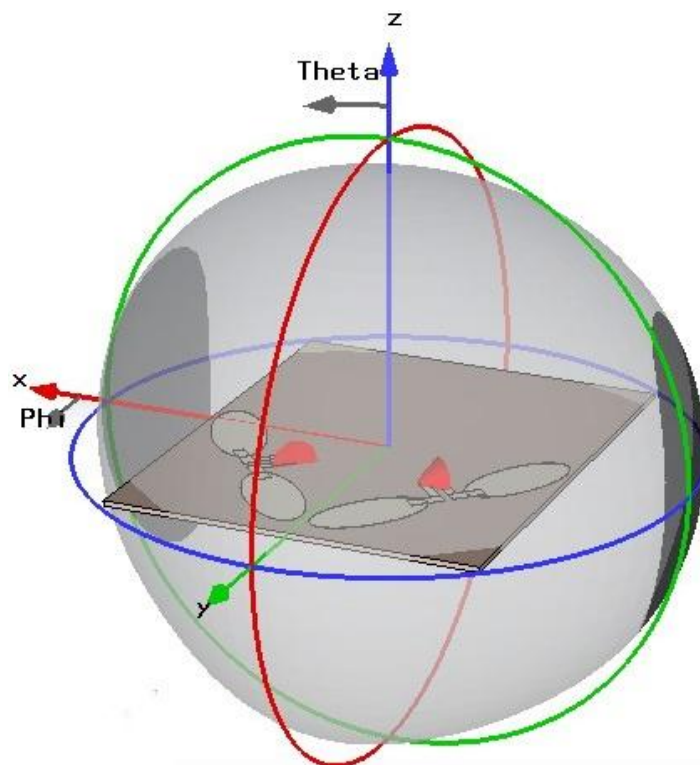


Figure 2: Spherical and Cartesian Coordinate systems

In addition to the 2D polar charts, 3D plots were used for the radiation pattern (Figure 2). One generic point in the spherical coordinate system is represented by the distance  $r$  and the angles  $\phi$  and  $\theta$ . The angle  $\phi$  describes the rotation angle in the azimuth plane ( $x$ - $y$ ) and  $\theta$  is the rotation angle in the elevation plane ( $z$ - $x/y$ ).

The design of the antenna models always follows the same rules in the Cartesian coordinate system:

- $y = 0$ : edge of the board
- $x = 0$ : middle of the board
- $z = 0$ : bottom face of the board

### **3.4 External influence factors**

All simulations were performed without and/or with different environmental influences, which are typical of the key:

- Without influence
- Battery
- Electronic components (ICs, LF-Tool,...)
- Package
- Body in front (Pocket)
- Body around (Human hand)

## 4 Concept studies and evaluation

The content of this chapter is the state of the art antenna analysis. The main focus is on wideband- and ultra wideband antennas. In addition, inherently to small bulkiness requirements, also miniaturization techniques for those antennas are investigated, in order to determine which kind of antenna structures better suit the electrical and geometrical constraints listed in the previous chapter and whose special implementation will be finally carried out in the next chapter. Based on the given specifications, three groups of antennas are suitable for this application:

- Dipole antennas
- Monopole antennas
- Planar Inverted-F antennas (PIFA)

For each one of these groups, suitable designs are summarized and compared with each other. Additionally, the advantages and disadvantages of the single analyzed configurations are pointed out. The main source for this research was the IEEE Xplore Digital Library [6].

For this UWB automotive application only planar, printed antennas are useful since they can easily fit into a small car key without occupying a big space. Therefore, all shapes shown for dipole- and monopole antennas are used for PCB printed antennas. The PIFAs are also mounted on PCBs, but in this case the radiator is printed on an additional ceramic block.

### 4.1 Dipole antennas

The basic antenna structure is a  $\lambda/2$  dipole antenna. The length  $L$  ( $= 2r$  in Figure 3) equals half the wavelength (2.3).

A  $\lambda/2$ -long thin-wire dipole is very sensitive to one frequency and has a narrow bandwidth. Therefore it is not useable for a broadband application. The radiator shape has to be modified to get a larger bandwidth. With increasing wire thickness, the usable spectrum of the antenna becomes larger. In the last decade a lot of different shapes for broadband applications have been reported in literature. These shapes basically tend to get as close as possible to a hemispherical shape. The more volume the radiator uses of the sphere, the higher the bandwidth will get.



Figure 3: Dipole antenna [3]

#### 4.1.1 Radiator shapes

The basic shapes for radiators are:

- Triangle ( $W$  (width),  $L$  (length))
- Rectangle ( $W$  (width),  $L$  (length))
- Ellipse ( $r_1$ ,  $r_2$ )

The wavelength of the antenna depends on  $L$ ,  $W+L$ ,  $r_1$  or  $r_1+r_2$ . These relationships vary with the radiator shape. Regarding the position of the different shapes of the radiator the antennas have different names. In the following part the main antenna shapes are described.

##### **Bowtie:**

The bowtie antenna is a planar version of a biconical antenna. The biconical antenna is one of the most commonly used broadband antennas and therefore the bowtie is also used very often. The main geometrical parameters of a bowtie antenna are represented by its length  $L$  and width  $W$ . Sometimes also the angle  $\alpha$  is used to describe the radiator in terms of angle aperture from the antenna center.

If the opening angle  $\alpha$  is increasing [7], also the bandwidth increases and the length gets smaller for the same frequency. The bowtie offers a great bandwidth. The matching circuit is more difficult than other dipole shapes [8]. The end of the radiator can be flat like in Figure 4 or rounded. In this case the antenna shape is also called fan.

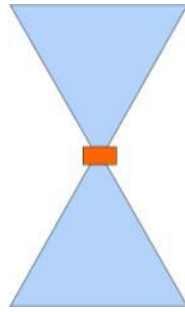


Figure 4: Bowtie dipole antenna [2]

**Diamond:**

By flipping the radiators of a bowtie antenna, it is possible to obtain a diamond antenna shape.

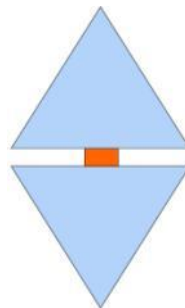


Figure 5: Diamond dipole antenna [2]

In the same way as for the bowtie antenna, also the diamond shape can be smooth on one side (in this case the side where the feed is connected to the radiator). In order to allow a smoother transition to the port impedance at the feed location, thus improving the matching bandwidth [9], the side of the triangle must be double rounded like in Figure 6.

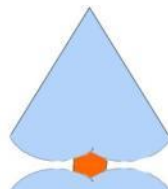


Figure 6: Rounded feed side diamond antenna

### Elliptical:

Elliptical antennas offer a wide bandwidth in combination with a fairly small size regarding the wavelength. A size reduction down to  $0.2 \lambda$  can be realized [10].

The geometrical parameters of an elliptical antenna are described by  $r_1 (= L)$  and  $r_2 (= W)$ . The ratio  $r_2:r_1$  is responsible for the bandwidth and the return loss  $S_{11}$ . The matching bandwidth improvements are quite significant for this shape [8].

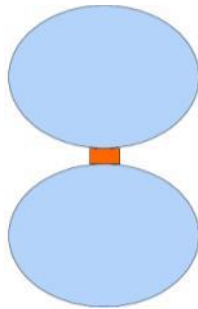


Figure 7: Elliptical dipole antenna [2]

An improvement in case of bandwidth and size reduction can be achieved by rotating the radiators with angles from  $20^\circ$  up to  $60^\circ$  [11].

By setting the size  $r_1=r_2$  a circular antenna is given.

### Rectangular:

The rectangular shape is like a very thick wire dipole, printed on a PCB. It is given by the length  $L$  and width  $W$ .

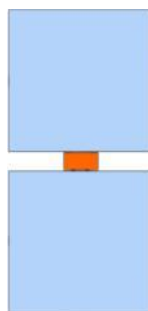


Figure 8: Rectangular dipole antenna

The rectangular shape can be optimized by changing the feed side to an elliptical shape or to a diamond shape (planar fat dipole). With these changes of the base one can combine the advantages of the diamond or the elliptical shape with those of the rectangular shape [7].

Another way to optimize the setting of a rectangular antenna is to displace the feed of the center or to realize a kind of loop antenna [12]. It is also possible to configure both radiators in a different length (asymmetrical dipole). This offset feeding technique enlarges the bandwidth and brings more flexibility for wideband impedance matching [13].

#### 4.1.2 Summary of printed dipole antennas

The previously listed dipoles are all used as UWB antennas in many applications and would fit our requirements in case of RF specifications. Furthermore, the radiation pattern of a combination of two dipole antennas would be an advantage to cover all directions of the key. Without special techniques for size reduction, the dimensions of these dipoles are too large to fit in the key.

In Table 1, the main performance indicators of dipole antennas are reported in dependence of the different shapes described in the previous paragraphs.

Antenna	Diamond	Elliptical		Rectangular	
Paper	[7]	[7]	[11]	[12]	[13]
$f_c$ [GHz]	-	-	3.8 , 8.9	2.7 , 5 , 8	3.15
Dimensions [mm <sup>2</sup> ]	40 x 15	40 x 14	50 x 34	34.2 x 16	40 x 5
$\epsilon_r$	-	-	3.55	-	2.2
BW [GHz]	3.8 – 8.8	3 – 20	3.1 – 10.6	2.87 – 10.04	2.91 – 3,38
$G_0$ [dBi]	-	-	3 – 5	-	-
Matching	good	good	-	OK	bad

Table 1: Comparison of dipole antennas

## 4.2 Monopole antennas

Monopole antennas use one radiator like the dipole antenna and the other one is realized as ground plane. The length  $L$  ( $= r$  Figure 9) is reduced to the quarter of the wavelength (2.6).

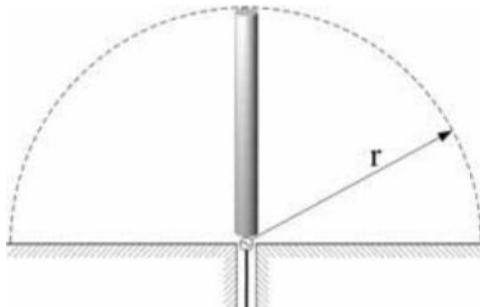


Figure 9: Monopole antenna [3]

In case of wideband properties the monopole antenna acts in the same way as the dipole antenna. For wideband applications the radiator has to be modified from a thin wire to other shapes.

### 4.2.1 Radiator shapes

The radiator shapes can be derived similarly as for the dipole antenna shapes. The dipoles as well as the monopoles will be manufactured as printed planar antennas. In Figure 9 the size of the ground plane is given by  $2r = \lambda/2$ . This means that in comparison to the dipole the monopole has no advantage as far as the size reduction concerns. How the ground plane and the associated feeding structure affect the whole antenna described in point 4.2.2.

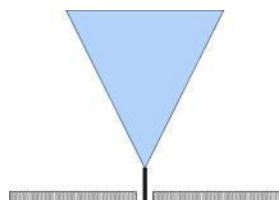


Figure 10: Bowtie monopole antenna

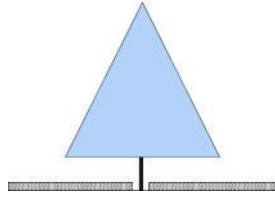


Figure 11: Triangular monopole antenna [2]

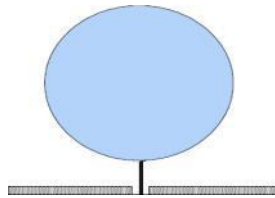


Figure 12: Elliptical monopole antenna

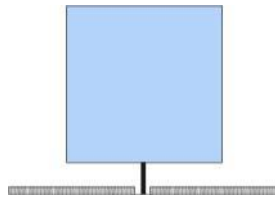


Figure 13: Rectangular monopole antenna [2]

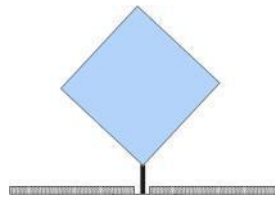


Figure 14: Diamond monopole antenna

#### 4.2.2 Feed and ground plane

Regarding printed antennas the ground plane can be designed in different ways. If the ground plane covers the whole space on the backside of the antenna substrate, the antenna type is a micro-strip antenna. For our use this kind of antenna is not suitable. Considering monopole antennas the ground plane can be built up with MS (micro-strip) feed or with CPW (co planar waveguide) feed. The choice of the feed that better suits the target specifications, depends on the shape of the radiators and on their dimensions. Also the length ( $L_1$ ) and width  $W$  of the ground plane vary with the shape of the antenna. The optimum size of the ground plane is  $\lambda/2$ , which is too large for our application. With

different techniques and for special shapes the size can be reduced. For example in case of the elliptical monopole antenna the ground plane can be decreased to around  $0.33 \lambda$  as discussed in [8], [14].

### MS feed:

The ground plane on the backside of the PCB covers the whole feed except a gap ( $g$  in Figure 15) to the radiator. The gap influences the bandwidth and the reflection factor of the antenna depending on the shape of the radiator. In general the MS feed monopoles provide better bandwidth performance ([14], [15]).

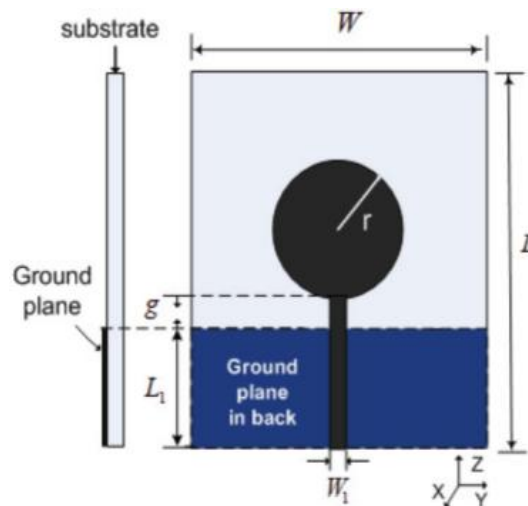


Figure 15: MS feed [15]

### CPW feed:

In case of CPW feed the ground plane is at the front side of the antenna. The gap  $c$  (Figure 16) between the feed and the ground plane is important for the impedance matching of the antenna to its feeding section. For  $50 \Omega$  matching the right ratio between  $W_1$  and  $c$  need to be found. For elliptical monopoles, the CPW feed provide better bandwidth performance, as described in [14], [15].

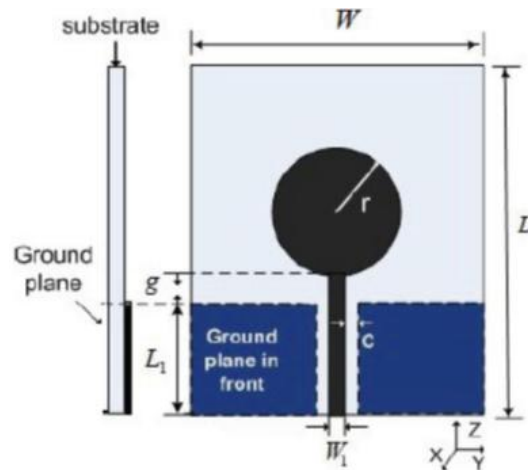


Figure 16: CPW feed [15]

One optimization tool special for CPW feed is to smooth the ground plane or to flatten them in the corner.

#### 4.2.3 Summary of printed monopole antennas

A comparison among monopole antennas with different shapes is shown in Table 2. The data are taken from published papers and they were scaled to the center frequency given for this project. All these data already consider the best cases and best optimization.

In spite of the size reduction of the radiator length to  $\lambda/4$ , the dimension for the whole antenna size is still quite large, especially because of the ground plane. Due to the given radiation pattern of a monopole antenna, at least two antennas have to fit in the key to cover all possible directions.

The main point for not using monopole antennas for the purpose of the thesis is therefore the ground plane. Some reasons led to this decision. The first point is the influence of the ground plane to the other electronic parts of the key. Furthermore because of the shielding due of the ground plane, a second monopole antenna would have been necessary on the backside of the key. The last main reason why monopoles do not represent a feasible solution for the purpose of the thesis is the available space due to the large ground plane. On the top side of the PCB the LF-Tool and the battery are next to the new system. On the back side are the control buttons and the loop antenna with its subsystems. Even if the electrical influence of the ground to the electronics could be controlled, there would be no space for a large enough ground plane neither on top nor on the back side of the PCB. Considering all these facts of an antenna array and the other applications, monopole antennas were found to be unsuitable for this system.

Antenna	Volcano smoke	Diamond	Elliptical			Rectangular	
Paper	[16]	[17]	[18]	[19]	[20]	[21]	[22]
<b>Dimensions [mm<sup>2</sup>]</b>	24.5 x 18	20 x 11	40 x 36	50 x 34	25 x 25	28 x 30	17 x 17
$\epsilon_r$	-	3.38	5.4	4.4	7.8	4.4	7.8
<b>BW [GHz]</b>	3.1 – 11.5	3.1 – 4.8	2.5 – 11.5	3 – 11.6	3 – 14	3.1 – 10.6	4.4 – 11.05
<b>G<sub>0</sub> [dBi]</b>	-	-	-	1.64	4.7	3.9	4.7
<b>Feed</b>	MS	-	MS	MS	MS	CPW	CPW

Table 2: Comparison of monopole antennas

### 4.3 Planar inverted antennas

The planar inverted antennas can be realized as inverted-L antenna or as inverted-F antenna.

#### 4.3.1 Inverted-L antenna (ILA)

The inverted-L antenna is a monopole antenna with one kink of 90°. The length of the radiator in z-direction is therefore reduced by the length of  $L$  (Figure 17). The total length of the radiator is still a quarter of the wavelength (4.1).

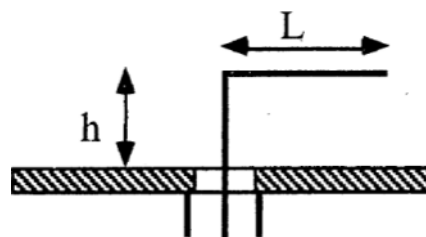


Figure 17: Inverted-L antenna [23]

$$\frac{\lambda}{4} = h + L \quad (4.1)$$

By adding a substrate in the free space between the ground plane and the radiator the length can be reduced further.

#### 4.3.2 Inverted-F antenna (IFA)

For the IFA the radiator is connected to the ground plane by a short cut. The length between the feed point and the short circuit is responsible for the impedance match of the antenna (Figure 18).

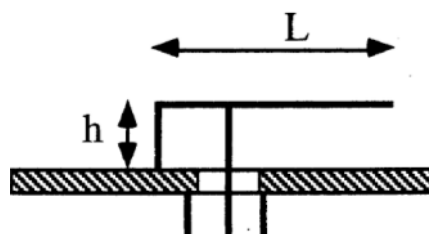


Figure 18: Inverted-F antenna [23]

In the same way as for a wire monopole, the width of the IFA has to be extended to increase the bandwidth. This antenna is called PIFA (planar inverted-F antenna). The parameters influencing the bandwidth are the length to width ratio, the height of the shortcut plane and the length of the shortcut.

The shortcut does not necessarily need to be extended along the whole side of the patch. By changing the length of the shortcut ( $W$  in Figure 19), the resonant frequency can be changed. In this case the position of the shortcut also influences the setting. The further away the feeding point is located from the shortcut, the easier the matching is. Moving the feeding point may result in a reasonable change of the resonant frequency too [24].

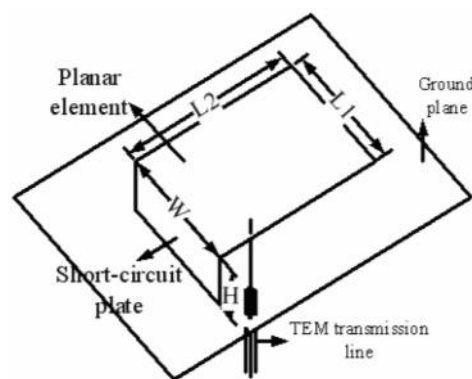


Figure 19: Planar inverted-F antenna [24]

$$\frac{\lambda}{4} \approx \sqrt{\frac{\epsilon_r + 1}{2}} (H + L1 + L2 - W) \quad (4.2)$$

The Equation 4.1 has to be adapted for planar inverted-F antennas and it results in Equation 4.2. The width  $L1$  (Figure 19) is influencing the wavelength in the same way as the length  $L2$ . The shortcut length and the height have also an influence on the center frequency [25].

The size and the shape of the ground plane have different effects on the antenna. Down to a ground plane length smaller than  $0.2 \lambda$ , the resonant frequency is barely influenced. For a ground plane length smaller than  $0.8 \lambda$  (for square shape) and  $0.4 \lambda$  (rectangular shape) there is no significant influence on the bandwidth. The gain is low for ground plane dimensions smaller than  $0.4 \lambda$ . Another significant influence is given for the antenna radiation pattern. A finite and small ground plane size introduces bad cross polarization ratio [26].

### 4.3.3 Summary of PIFAs

Planar inverted-F antennas are widely used for wireless communication in handsets like mobile phones. With special design techniques the size of these antennas becomes really small. Table 3 shows the characteristics of different PIFAs from the examined literature references. The designed named as “PIFA 1” provides UWB properties. The other two designs have been built up for ISM 2.4 GHz Wi-Fi band.

Nevertheless, the reduction, mostly done by increasing  $\epsilon_r$  or folding the radiators and/or the ground plane, has also some disadvantages and one worst one is the degradation of the radiation pattern properties of these PIFA antennas. To cover all directions around the key, four or six antennas would be necessary. Furthermore, a sufficiently large ground plane is essential for good performances of PIFAs. In the same way as for the monopole antennas, taking the other electronic subsystems of the key into account, a “big” and continuous ground plane is not a possible solution.

Antenna	PIFA 1	PIFA 2	PIFA 3
Paper	[27]	[24]	[28]
$f_c$ [GHz]	-	2.45	2.44
Dimensions [mm <sup>3</sup> ]	6 x 4 x 2.4	55 x 27 x 7.4	30 x 30 x 6
$\epsilon_r$	7.5	-	2.23
BW [GHz]	6.5 – 9.75	2.332 – 2.636	2.4 – 2.5
$G_0$ [dBi]	3.18	3	-
Matching	good	OK	OK

Table 3: Comparison of planar inverted-F antennas

## 4.4 Conclusions of the literature research

In this chapter, a number of different antennas configurations have been shown, most of them used for UWB or wideband applications. The advantage of the given specifications is the relatively large bandwidth of 1 GHz. This can be used in case of dipole antennas to scale down the proposed UWB antennas to smaller sizes, having as a result a narrower but still reasonably large bandwidth with a smaller shape.

All of these antennas are in their proposed shape and, especially in combination with a second or with more antennas, they are usually too large to fit in the assigned dimensions for the key. Some of them already use different miniaturization techniques to provide the smallest possible size and to maintain good bandwidth properties. Therefore, of the described structures can be already neglected for further implementation in this work. In particular, all monopole antennas and most of the PIFAs are not realizable in the environment of the application at hand because of their ground plane.

The miniaturization technique given by using high permittivity substrates is an easy way for size reduction. The drawback is that most of the antenna parameters deteriorate, such as impedance and bandwidth. Therefore, this way of down-scaling does not represent a promising approach for the purpose of this thesis.

Summarizing, this chapter should give an overview and in-depth analysis of possibilities to build up the antenna system for the application at hand. Several antennas would fit the given electrical specifications but they are not suitable for the integration into a small environment such as a car key. Therefore, only the following three antennas can be recommended:

- Elliptical dipole antenna with twisted direction of the radiators [11]
- Asymmetric rectangular dipole antenna [13]
- PIFA [27]

The next chapters will show the implementation of the three recommended antenna configurations for the specifications of this thesis work.

## 5 Implementation of miniaturized UWB dipole antennas

The result of the literature research done in Chapter 4 demonstrates that dipole antennas would fit best for the particular specifications given by this application. Of course, a standard dipole neither supports a large bandwidth nor is the structure very small. However the benefits of dipoles are:

- No ground plane is necessary
- Feed impedance ( $\approx 100\text{-}200\ \Omega$ ) match with input impedance of the IC

Especially the fact that no ground plane is needed is the main reason for choosing the dipole structure. This decision is based on the fact that other RF systems with different antennas are also implemented in this application. By using a large ground plane on one side of the print board, the other systems would be badly affected. Furthermore, the specification of a quasi-omnidirectional radiation pattern is hardly realizable with a large ground plane.

To fulfill the given specifications, the dipole structure has to be modified and a parametric analysis/optimization of the antenna is performed in this chapter. The aim of this section is namely an in depth study of the UWB dipole for a handheld device. The bandwidth needs to be broadened and the structure size needs to be reduced.

### 5.1 Stages of development

From the beginning particular attention was paid to miniaturized structures for broadband dipole antennas.

#### 5.1.1 Basic structure

One way to get a small structure is to design an asymmetric dipole. This means that the two radiators have a different length in case of a rectangular shape [13]. The asymmetrical shapes failed to produce the desired effect. Therefore, the design was changed to rounded front- and backsides to increase the bandwidth.

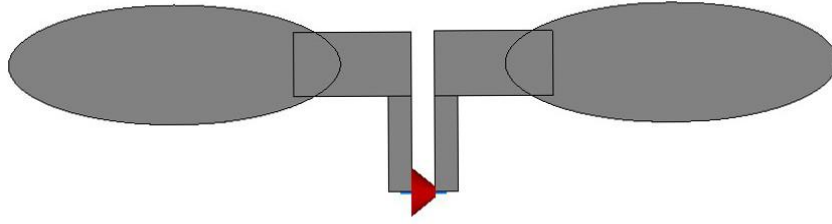


Figure 20: Elliptical dipole basic shape

After some simulations and adjustments the rectangular shape was completely transformed to an elliptical shape. This basic shape (Figure 20) fulfilled the RF specifications in regarding bandwidth, center frequency, the reflection coefficient and matching best in combination with its space requirement.

### 5.1.2 Miniaturization with permittivity $\epsilon_r$

Alongside with the miniaturization techniques by using different shapes, the substrate permittivity  $\epsilon_r$  can be used to reduce the size of the antenna. Special for printed antennas,  $\epsilon_r$  has a significant influence in combination with the height of the substrate. The size reduction is indirectly proportional to the square root of  $\epsilon_r$  [25].

$$f_c \sim \frac{1}{\sqrt{\epsilon_r}} \quad (5.1)$$

The permittivity does not only reduce the size, it affects the resonant frequency, gain, matching bandwidth and polarization. The performance and the physical shape decrease with increasing  $\epsilon_r$ .

The substrate material is given by  $\epsilon_r$  and the loss tangent  $\tan\delta$ . Starting with  $\epsilon_r = 1$  for vacuum, substrates are available up to  $\epsilon_r = 10$  or even more. A commonly used material is FR 4 ( $\epsilon_r = 4.4$ ,  $\delta = 0.02$ ) or e.g. Rogers 3210 ( $\epsilon_r = 10.2$ ,  $\delta = 0.003$ ). Simulations were done with different materials and different  $\epsilon_r$ . Rogers RO3206 delivered the best results and is used for all following simulations and also for the prototype manufacturing.

### 5.1.3 Double radiators

By adding a second dipole  $90^\circ$  rotated with respect to the other dipole, a quasi-omnidirectional antenna pattern can be realized. To keep the whole structure symmetric,

both antennas are rotated by  $\pm 45^\circ$ . The two antennas are located on the sides of an equilateral triangle on top of the given test board.

Due to the given board and its dimensions, it is necessary to reduce the size of the dipoles. The given space with 55 x 32 mm was not large enough to place the antennas along straight lines. One way to reduce the total length of the dipole is to rotate each half radiator by itself [11]. Unlike the results of the studies in paper [11], in this design the radiators are rotated unequally. The top radiators are rotated by  $20^\circ$  and the bottom radiators by  $35^\circ$ . In this way the used space in x-direction gets minimal and thus the space between the two antennas maximal. The larger the space between the antennas, the smaller the influence from one to the other is. Because of the unequal rotation, the antenna shapes get asymmetrical. However, the influence is negligibly small. The final shape is shown in Figure 21 and was only adapted for different matching impedances.

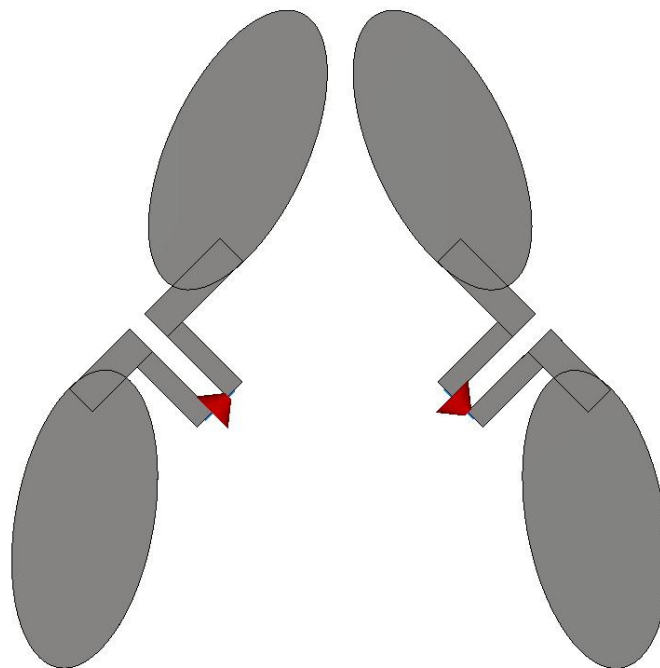


Figure 21: Double elliptical dipole for 200  $\Omega$

#### 5.1.4 Input impedance

This basic configuration is designed for 200  $\Omega$  and the given specifications. For the same board size the antennas were adapted to 50  $\Omega$  and 100  $\Omega$  (differential impedance). The 100  $\Omega$  differential input impedance corresponds with 50  $\Omega$  single ended. This impedance is used in the measurement chamber and for the whole measurement equipment, which is normalized to 50  $\Omega$ .

The impedance of the antenna is set with the gap size  $g$  between of the feeding line (Figure 22). By changing this parameter, the whole antenna needed to be adapted slightly. In Table 4 the different settings are shown for the different final designs and different input impedances.

## 5.2 Simulations

The settings for CST Microwave Studio and a short description for the measurements are mentioned in chapters 2 and 3. In this part the results are shown and discussed.

### 5.2.1 Parameters

In CST all variables of the different shapes are parameterized. The used variables of the antennas (Figure 22) and the final values are shown in Table 4.

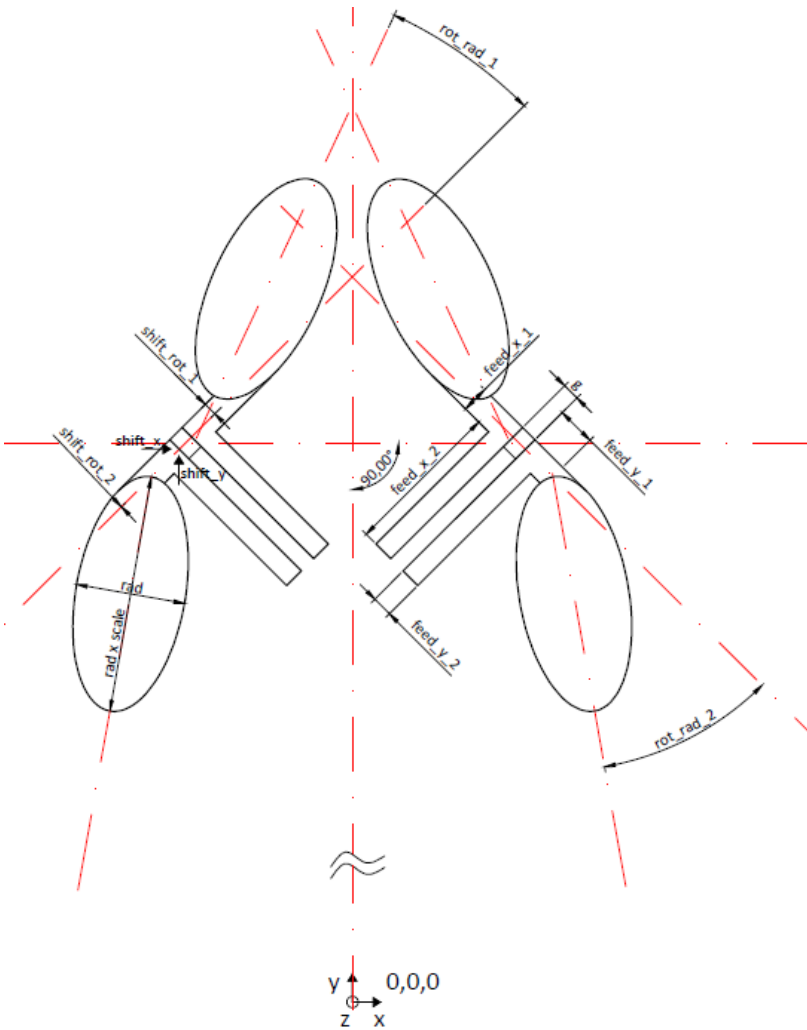


Figure 22: Double dipole parameters

Variable		Input impedance			Description
		50 $\Omega$	100 $\Omega$	200 $\Omega$	
<i>g</i>	mm	0.2	0.5	1	Differential feed gap
<i>rad</i>	mm	6.5			Width of the radiator
<i>scale</i>		1.7	2	2.18	$rad * scale = \text{length of the radiator}$
<i>rot_rad_1</i>	$^{\circ}$	-20			Rotation of the top radiator
<i>rot_rad_2</i>	$^{\circ}$	-35			Rotation of the bottom radiator
<i>shift_rot_1</i>	mm	1.5	1.5	2	Shift out of the feed center of the top radiator
<i>shift_rot_2</i>	mm	0	0	0	Shift out of the feed center of the bottom radiator
<i>feed_x_1</i>	mm	1.5			Feed 1 width
<i>feed_y_1</i>	mm	2			Feed 1 length
<i>feed_y_2</i>	mm	1			Feed 2 width
<i>feed_x_2</i>	mm	4			Feed 2 length
<i>shift_x</i>	mm	9			Antenna shift out of $x=0$ position
<i>shift_y</i>	mm	40	40	39	Antenna shift out of $y=0$ position
<i>metal_h</i>	mm	0.035			Metal height
<i>sub_x</i>	mm	32			Dimensions of the PCB substrate
<i>sub_y</i>	mm	55			
<i>sub_h</i>	mm	0.635			

Table 4: Dipole antenna parameters

The following documented simulation results consider the 200  $\Omega$  design. As mentioned in Chapter 3, the simulations consider the antenna itself and the antenna influenced by other parts on or around the PCB.

## 5.2.2 Reflection coefficient $S_{11}$

Figure 23 shows different  $S_{11}$  for the isolated antenna (D12) only in the presence of the second dipole terminated with a matching load and for the same double antenna configuration with different impacts on board. D12+B displays the influence of the battery and D12+I the impact of an IC placed next to the antennas. Also a combination of both is shown in D12+B+I. As seen in this chart,  $S_{11}$  is not badly influenced by these PCB mounted parts.

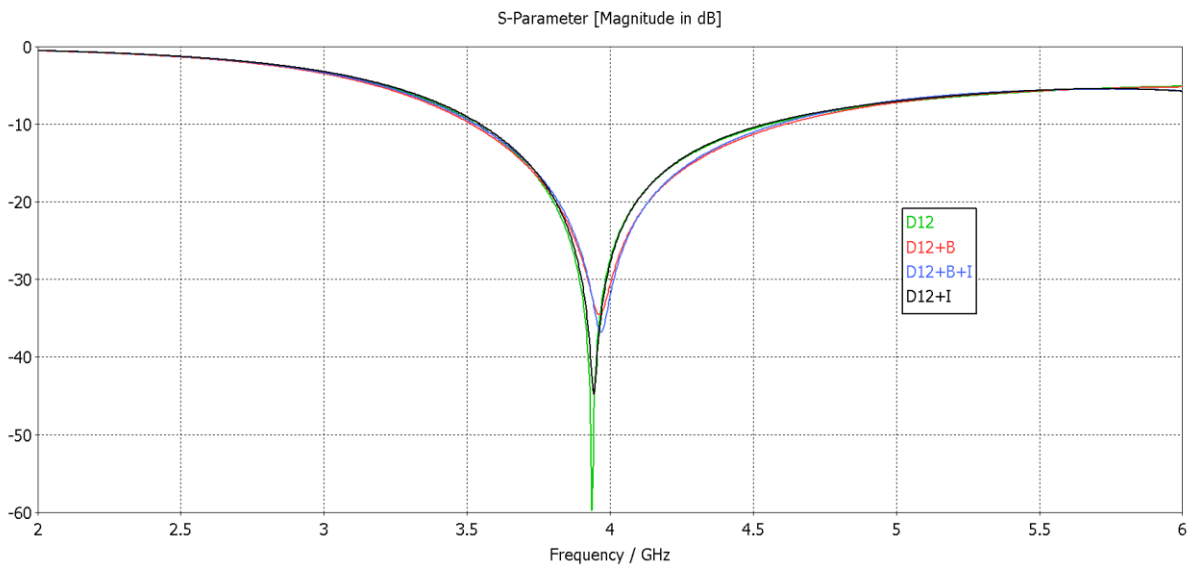


Figure 23:  $S_{11}$  comparison for PCB parts

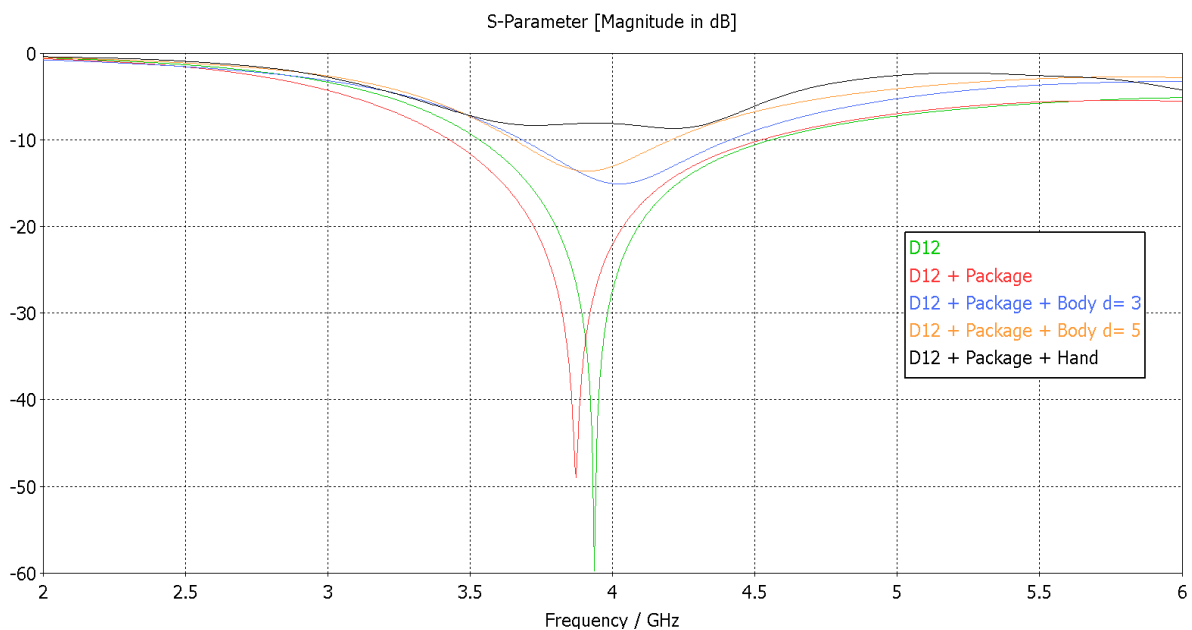


Figure 24:  $S_{11}$  comparison for PCB surrounding

D12 is also used as best case reference in Figure 24. In this chart the curves show the effects of a human body behind the key (D12+Package+Body). The graphic D12+Package+Hand shows  $S_{11}$  with the key being held in a hand. The material used for the body is a high-loss high permittivity substrate synthesized by the typical following specifications:

- Relative permittivity  $\epsilon_r = 31.29$
- Electrical conductivity  $\sigma = 8.0138 \text{ S/m}$

These values correspond with a human skin tissue. The hand is simulated as a cylinder with an outer diameter of 6 cm, an inner diameter of 4 cm and a length of 10 cm (Figure 25). The human body is simulated with a brick of 40 cm x 40 cm x 10 cm. The key is positioned at a distance of  $d = 3 \text{ mm}$  or  $d = 5 \text{ mm}$  away from the body.

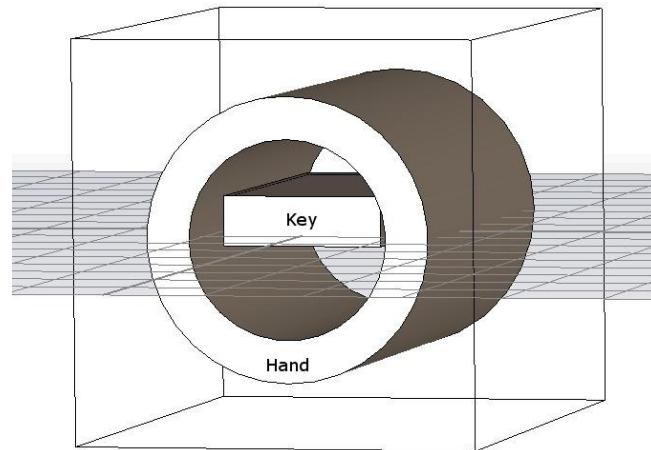


Figure 25: Key in hand simulation design

In addition to the hand and the body simulations, the key plastic package was taken into account. The package itself has a minor influence on the antenna. As far as the hand and body are considering in the simulations, however, the  $S_{11}$  significantly worsens. The simulation of the key in the hand shows a degradation of the minimum of  $S_{11}$  to -8 dB. This means that the antenna gets out of tune badly by putting it next to or by surrounding it with human tissue.

Given by the predefined dimensions of the key PCB, all former simulations were optimized for a 32 mm wide board. This limitation resulted in the antenna properties shown in Figure 24 and 27. The next graph (Figure 26) represents  $S_{11}$  for different radiator rotations. By

reducing the angles  $rot\_rad\_1$  and  $rot\_rad\_2$ , the total size of the antenna group increases and with it the board width  $sub\_x$ .

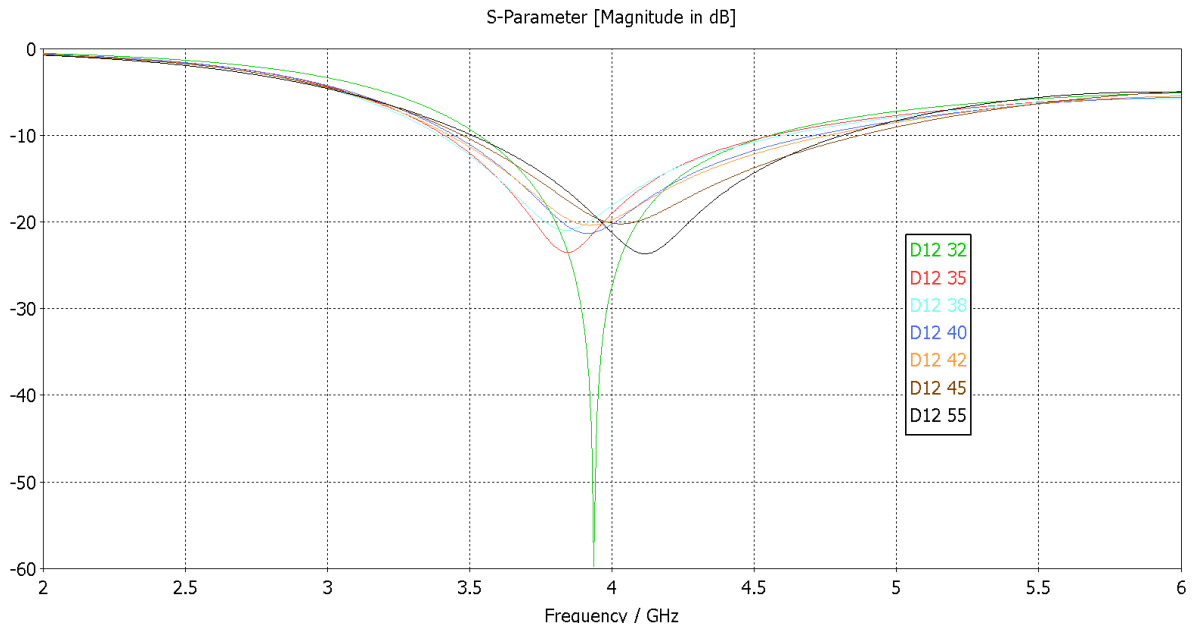


Figure 26:  $S_{11}$  comparison for different radiator rotations (legend see Table 5)

In Table 5, the different settings are mentioned. For optimization reasons, the shifts of the minima ( $shift\_rot\_1$ ,  $shift\_rot\_2$ ) were also changed. In the case of  $S_{11}$ , all settings fulfill the specifications. The reason for this investigation is apparent in the antenna patterns in Figure 29.

graph	$sub\_x$	$rot\_rad\_1$	$rot\_rad\_2$	$shift\_rot\_1$	$shift\_rot\_2$
	mm	°	°	mm	mm
green	32	-20	-35	2	0
red	35	-12	-27	4	-0.5
turquoise	38	-8	-20	8	-1.75
blue	40	-6	-17	12	-2
orange	42	-5	-15	12	-2
brown	45	-5	-15	2	0.3
black	55	0	0	0	0

Table 5: Comparison of different board sizes and radiator angles

### 5.2.3 Coupling coefficient $S_{12}$

Next to the simulations for the reflection coefficient  $S_{11}$  also the coupling coefficient  $S_{12}$  was under investigation. The following three figures show  $S_{12}$  with the same simulation settings as for the  $S_{11}$  simulations before.

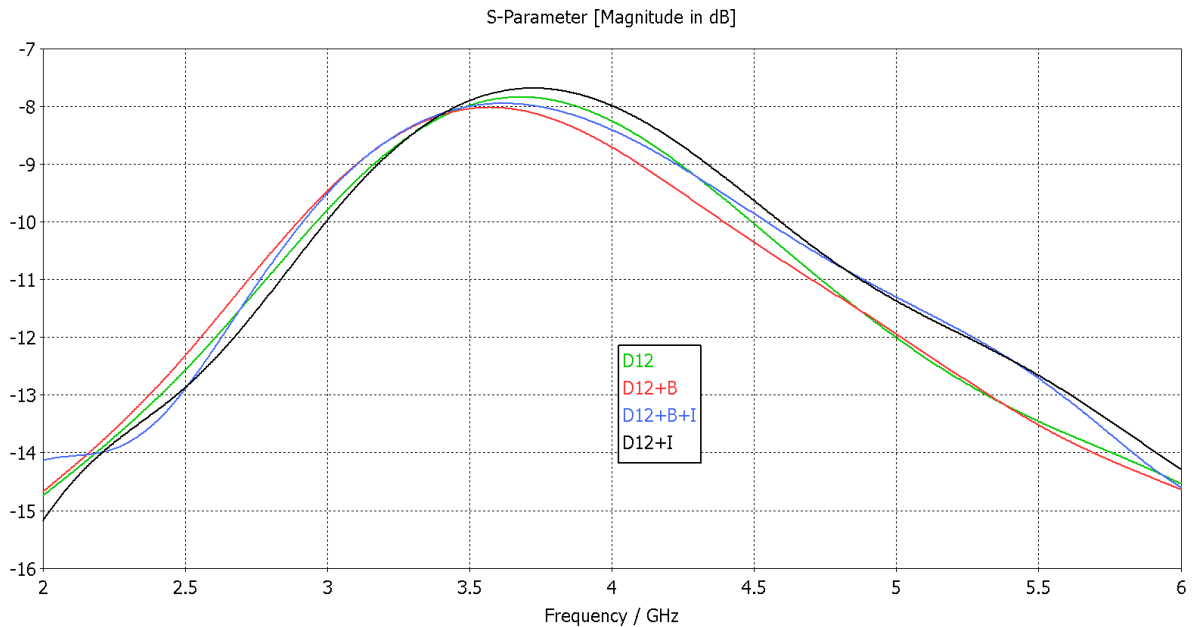


Figure 27:  $S_{12}$  comparison for PCB parts

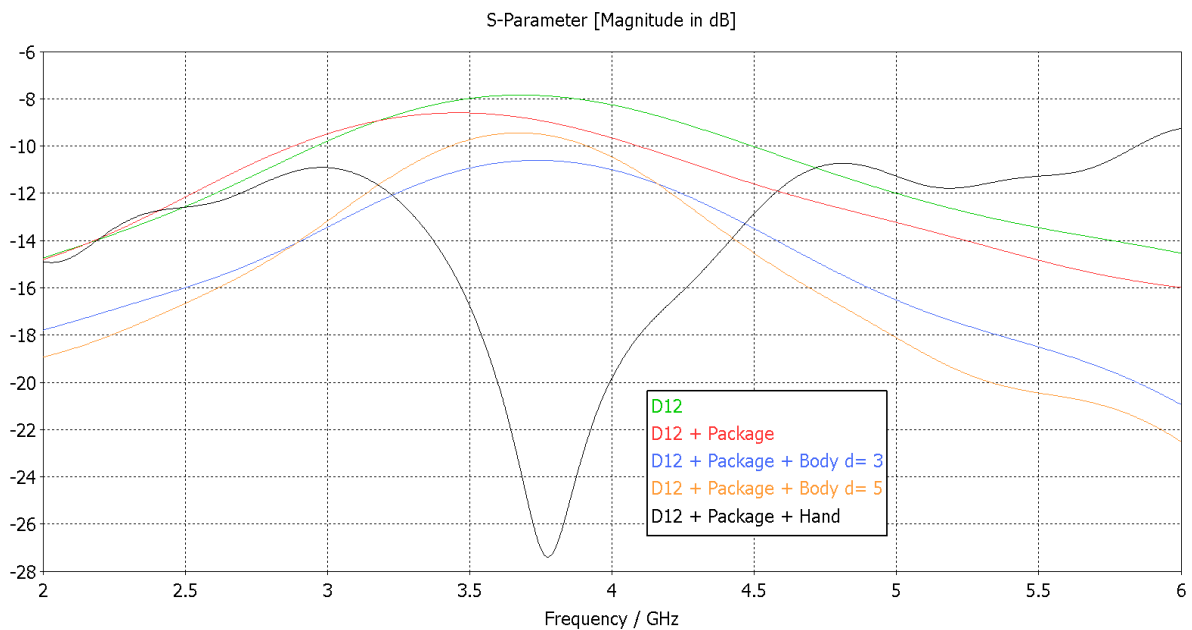


Figure 28:  $S_{12}$  comparison for PCB surrounding

In Figure 27 the influence of PCB mounted electronic devices on  $S_{12}$  is shown. The variation of the graphs for the different  $S_{12}$  is very small, regarding to the influences caused on other antenna parameters. The coupling factor is around -8 dB to -10 dB in the used spectrum. These values are hard on the edge for a functional transmitting- and receiving system.

Related to the power losses given by the human tissues next to the antennas, also  $S_{12}$  decrease for these simulation parameters (Figure 28).

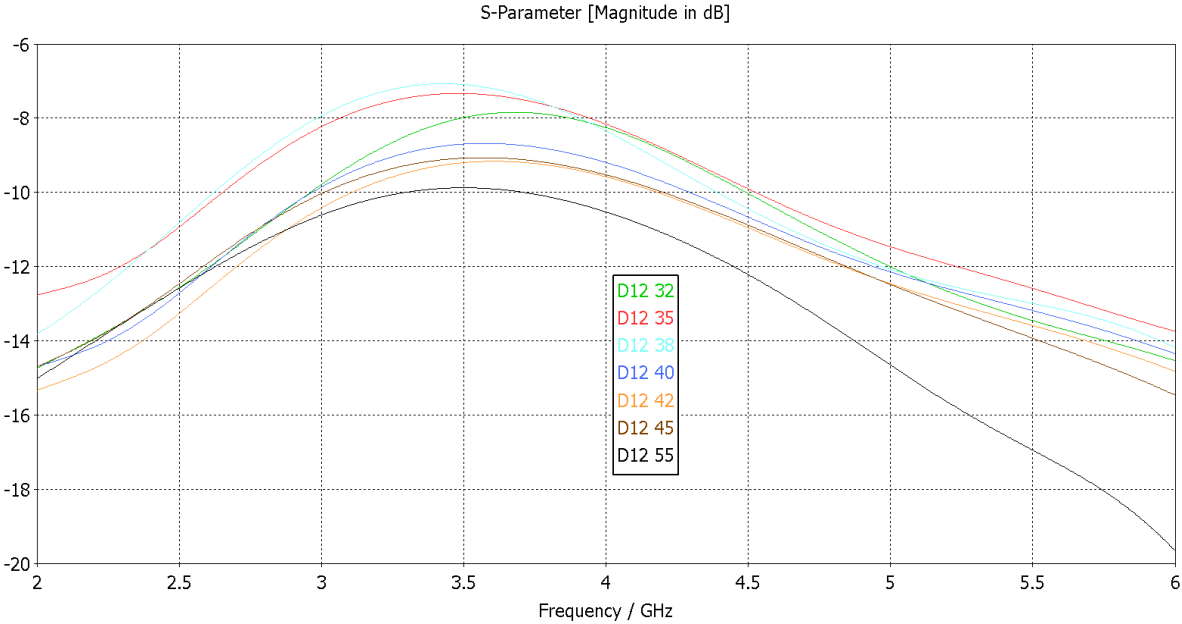


Figure 29:  $S_{12}$  comparison for different radiator rotations (legend see Table 5)

Figure 29 shows the influence of different rotation angles for the dipoles on the coupling between the two dipoles. The coupling factor is not only related to the board size or the rotation angle. The smaller the rotation angle is, the smaller the area of both dipoles facing each other. But the major impact is given by the distance between the two top radiators. Therefore,  $S_{12}$  is relatively high for the board size of 35 mm and 38 mm (Figure 29: D12 35, D12 38) caused by the packed design.

The reason for the investigation of the isolation coefficient  $S_{12}$  is the importance of this parameter regarding a good interaction of the antenna with its subsystem. Caused by a too high coupling between the antennas the whole system is disturbed. In this case the IC is not able to differentiate the received signal if it is a coupling signal from the other antenna or a signal from outside the key.

## 5.2.4 Antenna pattern

All figures use a different scale starting with +3 dB to emphasize the differences. For all antenna patterns the green curve is used as reference curve. Apart from Figure 30, this curve shows D12 at 4 GHz and the given requirements from Paragraph 1.2.

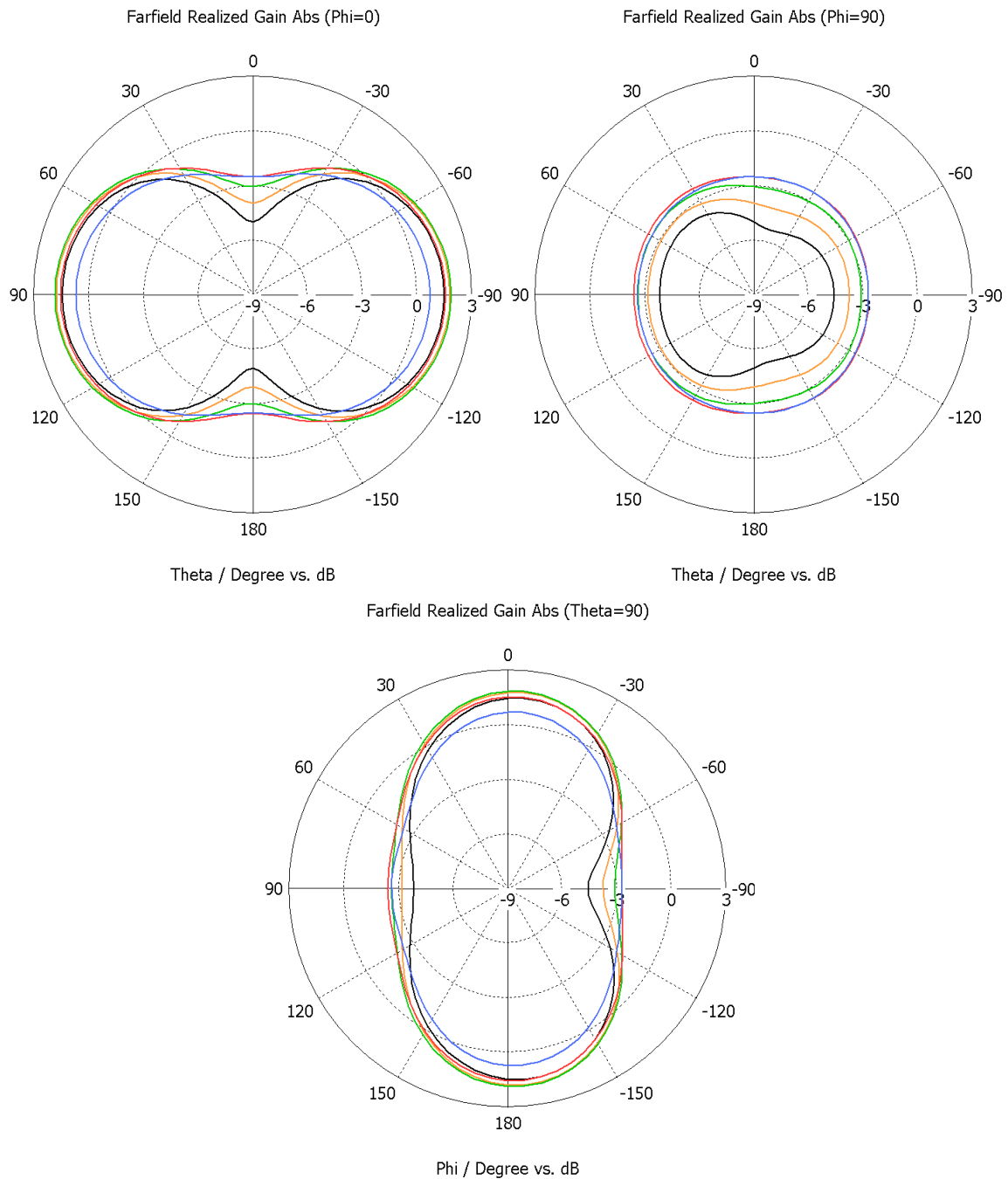


Figure 30: Far-field plot with D12 for different frequencies:

3.5 GHz (blue), 3.75 GHz (red), 4 GHz (green), 4.25 GHz (orange), 4.5 GHz (black)

In Figure 31 the common realized gain of the double dipole (both antennas are fed at the same time) D12 is shown. The curves describe the radiation behavior for different frequencies in the used bandwidth from 3.5 GHz to 4.5 GHz in 0.25 GHz steps. If we compare the five curves, we recognize the increasing minima in all three plots. The minima increase with the frequency. This is caused by a different frequency phase-dependence in the addition operation of the radiation pattern associated to the single antennas. This effect can be identified also for Figure 31 and later in the antenna gain plot (Figure 35).

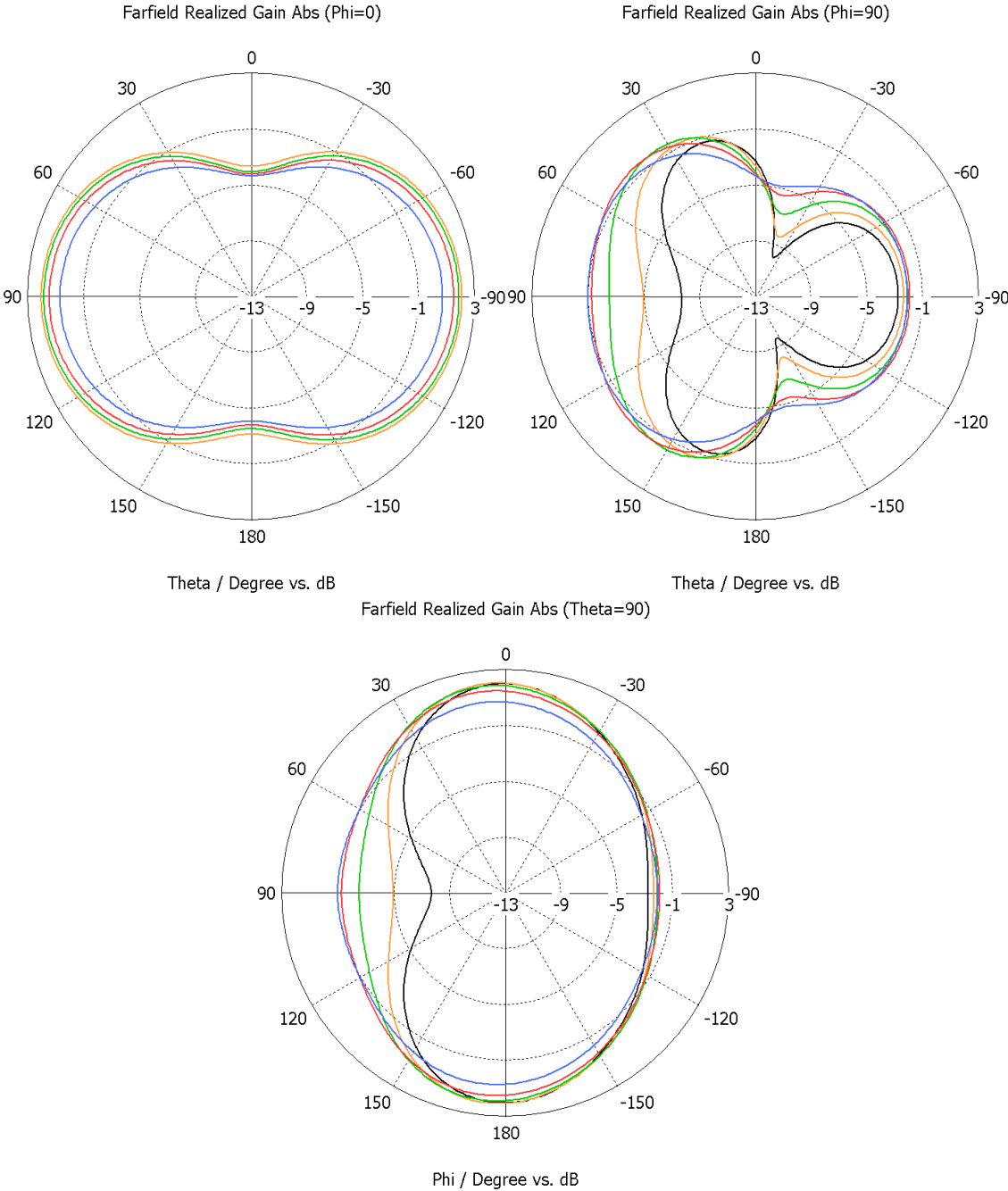


Figure 31: Far-field plot with D12 and battery for different frequencies:  
 3.5 GHz (blue), 3.75 GHz (red), 4 GHz (green), 4.25 GHz (orange), 4.5 GHz (black)

The battery with its given dimension (Paragraph 1.2) is the biggest metal part next to the antennas on the PCB. Therefore, its impact on the antennas was under special investigation. The diagram in Figure 31 was obtained through the same simulation setup as the result in Figure 30 with the addition of the battery. Due to reflection introduced by the battery, the maximum of the radiation pattern moves into the y-direction and two minima arise.

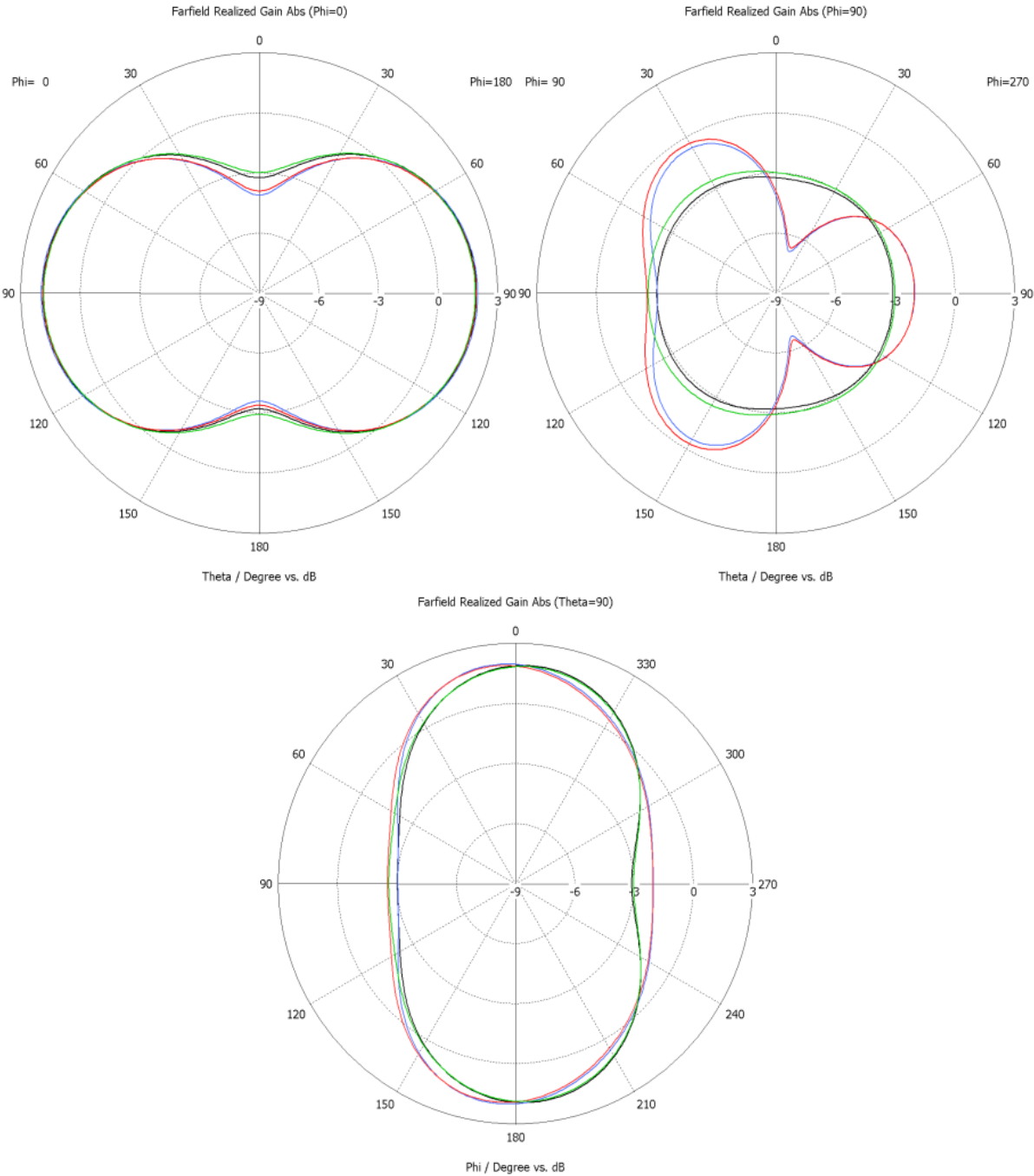


Figure 32: Far-field plot of the double antenna with PCB disturbances:

D12 (green), D12+B (red), D12+B+I (blue), D12+I (black)

Similarly as for  $S_{11}$ , Figure 32 and 33 the effects on the radiation pattern of PCB-sub-modules and human body parts. Figure 34 shows the realized gain pattern for different radiator rotations.

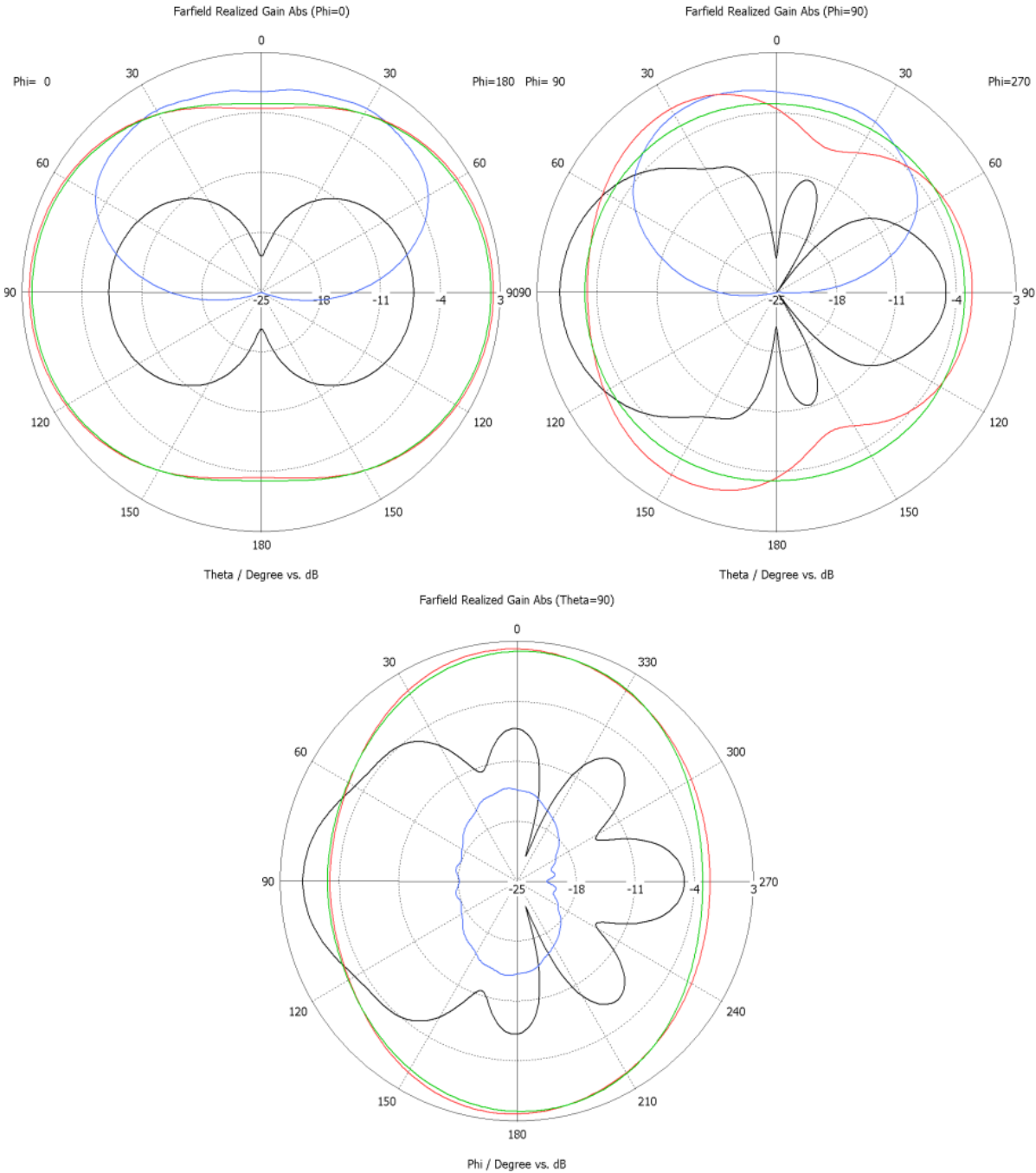


Figure 33: Far-field plot for PCB surrounding:

D12 (green), D12+Package (red), D12+Package+Body (d=3=5 blue), D12+Package+Hand (black)

Compared to the  $S_{11}$  case, the impacts of the PCB mounted parts become more evident in the radiation patterns as shown in Figure 34. As mentioned before, the battery has the biggest effect on the antenna radiation properties. Therefore, also for the following simulations the battery is considered. The impact of an IC next to the antennas is smaller than expected and can be neglected.

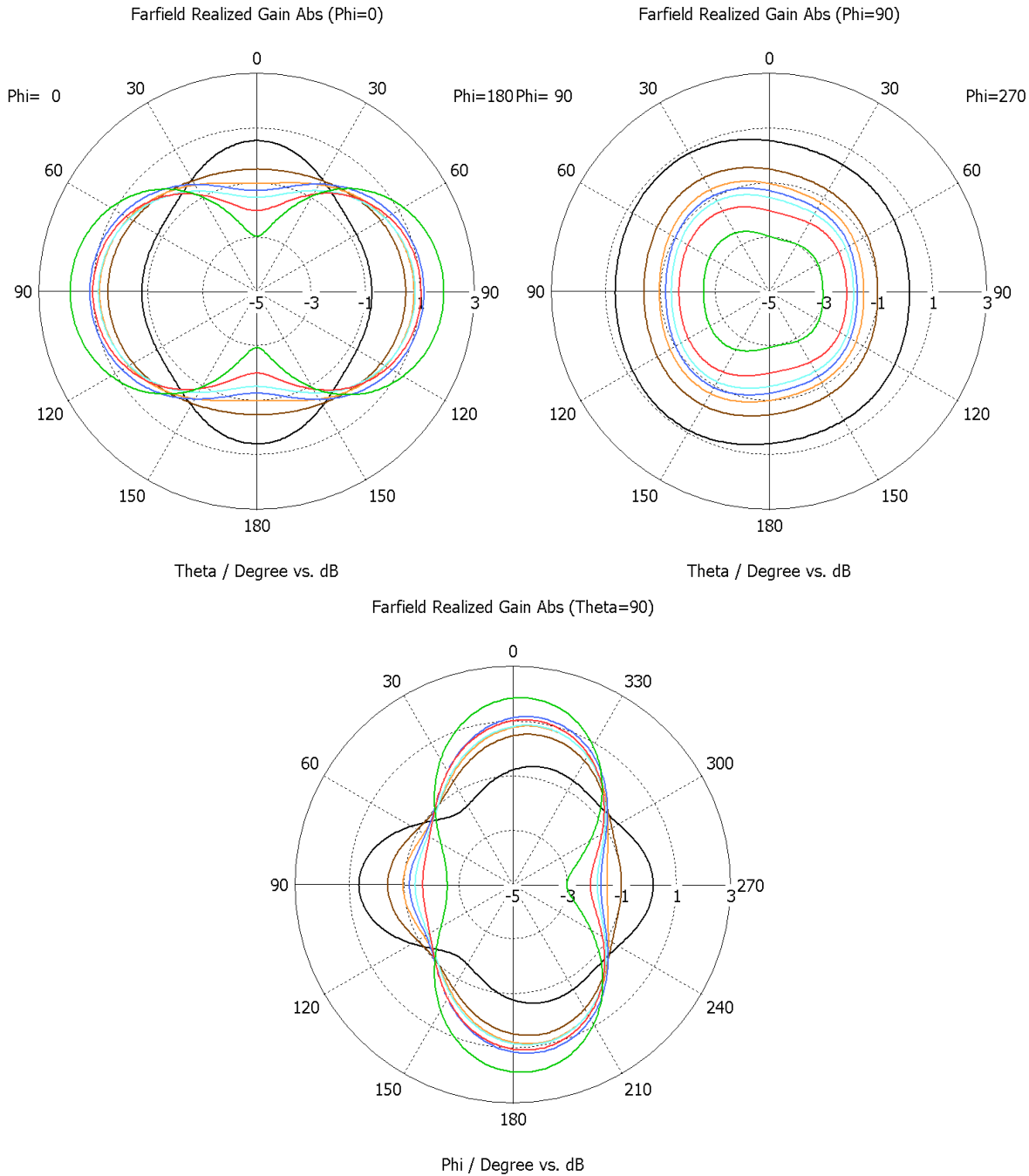


Figure 34: Farfield plot for different radiator rotations (for the legend see Table 5)

In another simulation run, the place of the battery was varied. The battery was shifted from the top layer to the bottom layer and also closer or more far away from the antennas. The cognition out of this simulation is that the influence is indirectly proportional to the distance of the battery to the antennas. In what way the distance increase ( $y$ -,  $z$ - or both directions) is insignificant.

Of course also the size of the battery is important. A smaller battery causes lower influences. Because of the huge amount of systems, used in this key, the battery has to deliver a certain power. For this voltage and current only a battery with the given size is available.

In Figure 33 the effects of a human body become evident. In case of a person next to the key, the body acts like an absorber due to the high loss tangent and permittivity. The body absorbs all energy in his direction and hardly any energy can travel through. The distance  $d$  between the body and the key is negligible. For the simulations with only the hand (Figure 33, black curve) the results are slightly better, but the attention in the worst case reaches 25 dB.

One of the goals of this thesis is to investigate and design an omnidirectional antenna for a key application. In Figure 34 the quasi-omnidirectional property is shown for different sizes of the PCB board. With the increase of the width of the board, the rotation angles can be reduced and the dipoles become straighter. It can be Figure 34 that the radiation pattern becomes more omnidirectional. In case of straight dipoles with rotation angles of zero, the pattern varies over the whole sphere with only 1 dB. A good compromise of used space and quasi omnidirectional pattern, offer the turquoise or blue curve. As seen in Table 5 the board size for these simulations are 38 mm and 40 mm. The variation of the gain is 1.5 dB.

### 5.2.5 Antenna gain

The antenna gain changes with the angle and the frequency. Depending of the direction, the gain variation lies between 1 dB and 1.5 dB. The dashed lines represent the gain for the antennas with battery. In this case the variation rises up to 7 dB in worst case for one direction. This phenomenon is also visible in Figure 32. In Figure 35 the gain is plotted for three directions. The red curves represent the  $z$  direction, the green curves the  $x$  direction and the blue curves the  $y$  direction.

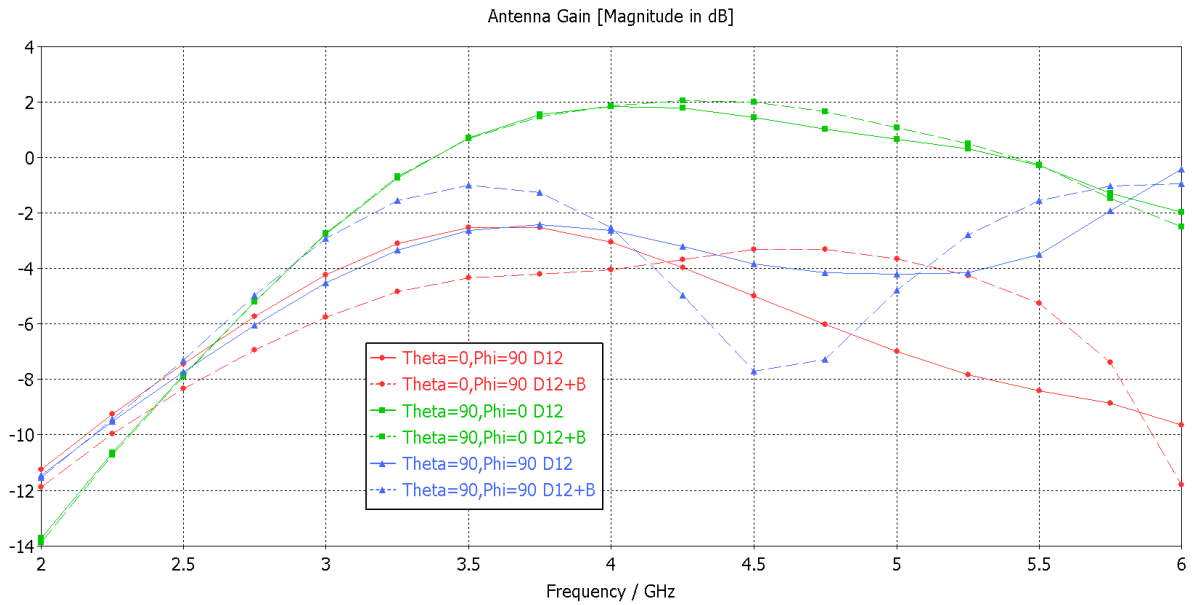


Figure 35: Antenna gain with or without battery

### 5.2.6 Group delay

The only positive effect of the battery is visible in the group delay  $\tau_g$ . Within the used bandwidth the group delay has a variation of 0.01 ns for the single antenna (Figure 36 green curve) and a variation of 0.005 ns by taking the battery into account (Figure 36 red curve). This influence is not important, because even the 0.01 ns are very not significant in terms of group delay.

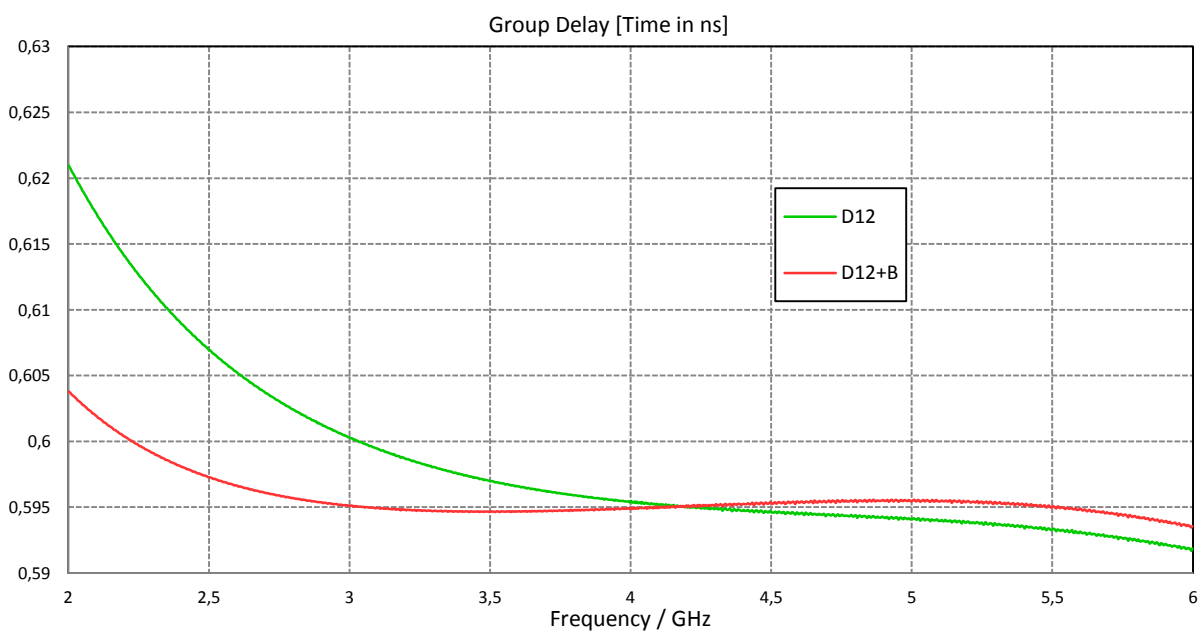


Figure 36: Group delay with or without Battery

## 5.2.7 Cross-polarization ratio

The result of the cross-polarization simulations are shown in Figure 37. The values correspond to the ratio of a field probe in  $y$  direction to a field probe in  $x$  direction. Every probe pair was placed at far-field distance around the PCB. Due to the asymmetrical position of the antenna pair on the board, the results of the negative and positive direction are not equal. According to the direction, the cross-polarization ratio varies with the frequency.

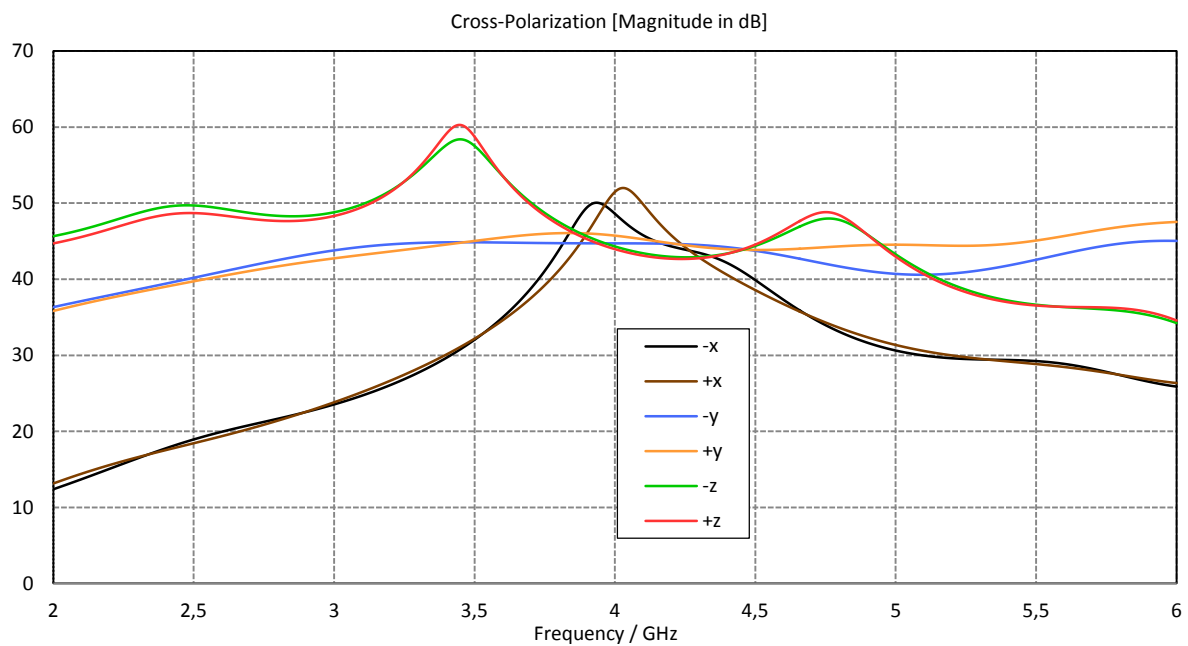


Figure 37: Cross-polarization in different directions

Excluding the  $x$ -direction the difference between the main field and its orthogonal field is 45 dB or higher over the used spectrum. In case of the  $x$ -direction the variation of the ratio is higher than for the others starting with 33 dB.

### 5.3 Prototype manufacturing

To achieve a high level of variability in the measurements and to simplify the measurements three different designs with different ways for the connection were designed.

The first design is the standard antenna (Figure 21). This design was adapted to two other designs with via holes for a backside feeding. The via holes are placed on the front end of the feeding structure. The difference between those two designs is the distance between the via holes. In one case the holes are placed right in the middle of the feed with a drill of 0.8 mm. In the second case the gap between the wholes got increased and the drill was 1.2 mm for an easier connection of measurement cables or connectors. Each of these three feeding possibilities were designed for a differential input impedance of 50 Ω, 100 Ω and 200 Ω.

In total 9 designs were exported as Gerber-files and placed on a Rogers RT3206 PCB with a size of 12 x 8 inch. Due to the small antenna size, a minimum of 55 prints could be manufactured on one single laminate (Figure 38).

The final PCBs were drilled and gold plated against oxidation and to increase the conductivity of the transmission line.

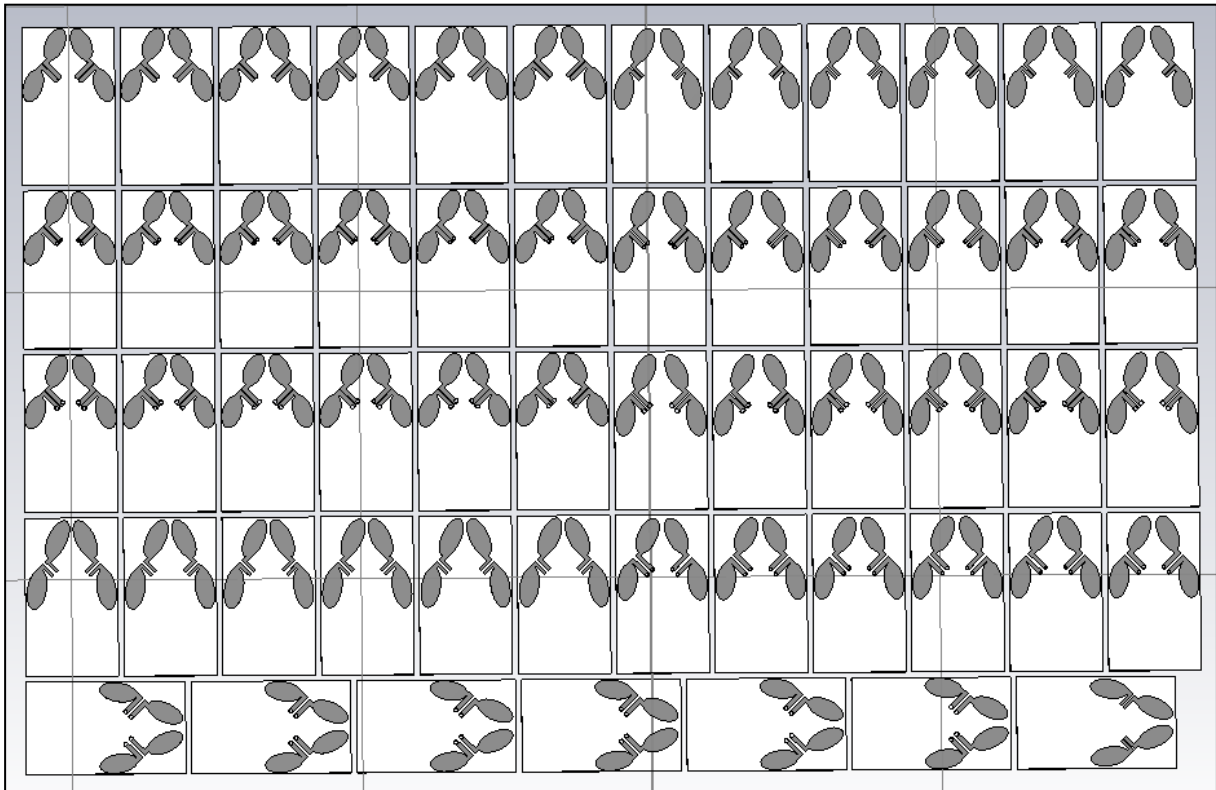


Figure 38: Gerber-file for PCB production

## 5.4 Measurements

In this chapter the measurement results are documented, analyzed and compared to the simulation results.

The measurements were performed in the local high frequency laboratory and in the high frequency anechoic chamber. The laboratory is a dedicated clean room (ISO 7 / class 10,000) with controlled air temperature and humidity. The measurement chamber has a dimension of 5 m x 5 m x 4.5 m and it is equipped with two independent near field scanners. It is designed for measurements from 400 MHz up to 20 GHz [29].

The following points describe the used equipment, the connection techniques and the results.

### 5.4.1 Measurement equipment

For all measurements the Rohde&Schwarz Vector Network Analyzer ZVA24 (Figure 39) was used. This network analyzer is a four port analyzer with a usable frequency from up to 24 GHz. For every measurement, the analyzer with its measurement cables were calibrated with the Rohde&Schwarz Calibration Kit ZV-Z52 (10 MHz - 24 GHz). The analyzed frequency spectrum was set from 2 GHz to 6 GHz as for the simulations. The following settings were used for the measurements:

- Start frequency: 2 GHz
- Stop frequency: 6 GHz
- Step size: 10 MHz
- Power level of the internal source: 0 dBm

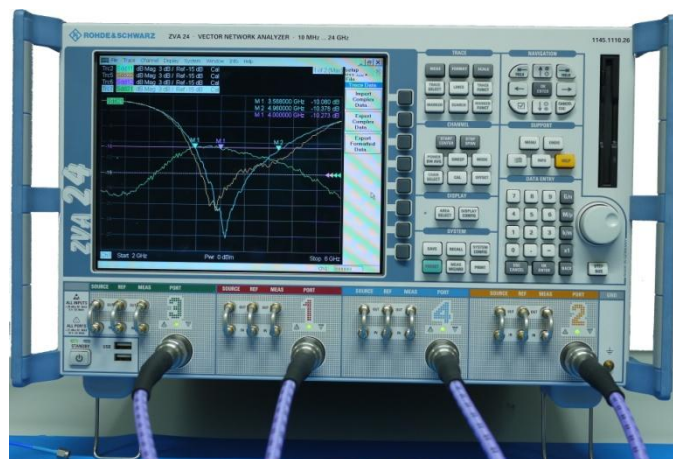


Figure 39: Rohde&Schwarz Vector Network Analyzer



### 5.4.3 Reflection coefficients $S_{11}$ and $S_{22}$

The S-parameters were measured with a special function of the network analyzer. Therefore, two ports were coupled together as one balanced port. Port 1 and port 2 were used for the right dipole and port 3 and 4 for the left dipole. The measurement cables were directly connected to the four soldered semi rigid cable on the board (Figure 41).



Figure 41: S-parameter measurement

With a rectangular window  $S_{11}$  and  $S_{22}$  could be plotted as shown in Figure 42. Caused by the inaccuracies of the length of the semi-rigid cables,  $S_{11}$  is slightly different from  $S_{22}$ .

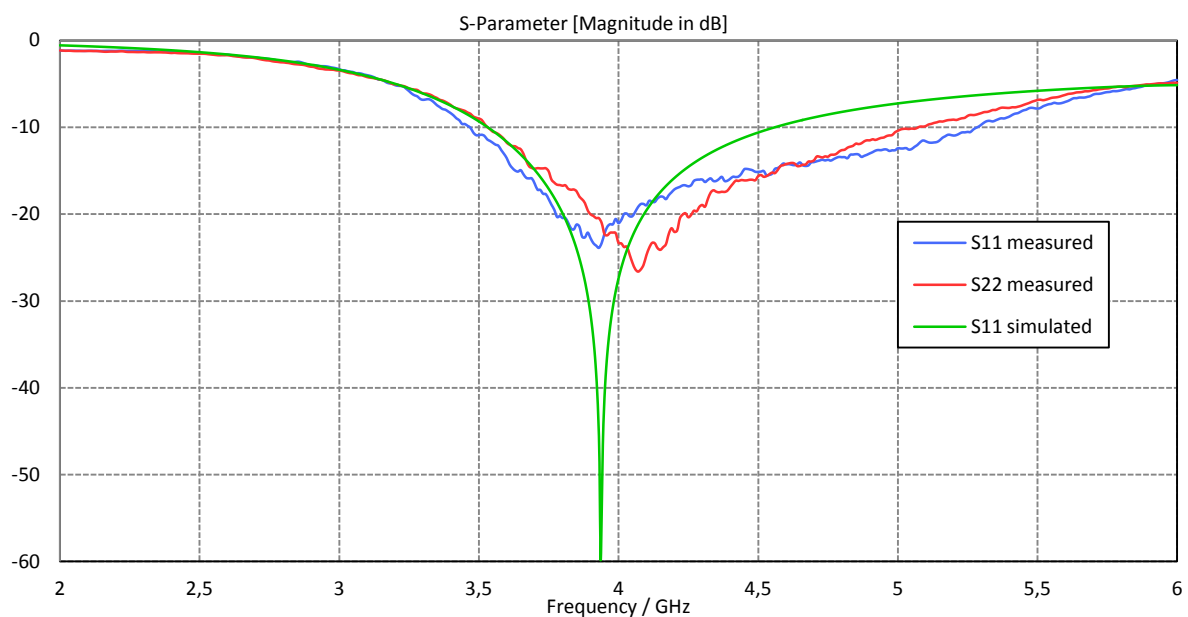


Figure 42:  $S_{11}$  and  $S_{22}$  measured and simulated

In comparison to the simulation charts of  $S_{11}$  and  $S_{22}$  (in the simulation  $S_{11} = S_{22}$ ), the manufactured antenna has a higher bandwidth (BW = 1.5 GHz), but the minima of the reflection coefficients of both dipoles are slightly shifted in frequency with respect to the original from 4 GHz center frequency.

The differences between the simulation results and the measurement results are caused by tolerances of the used connection to the measurement equipment and the tolerances of the manufacturing. Nevertheless, the given specifications are fulfilled.

#### 5.4.4 Coupling coefficients $S_{12}$ and $S_{21}$

Out of the measured S-parameter  $S_{12}$  and  $S_{21}$  can be plotted too.

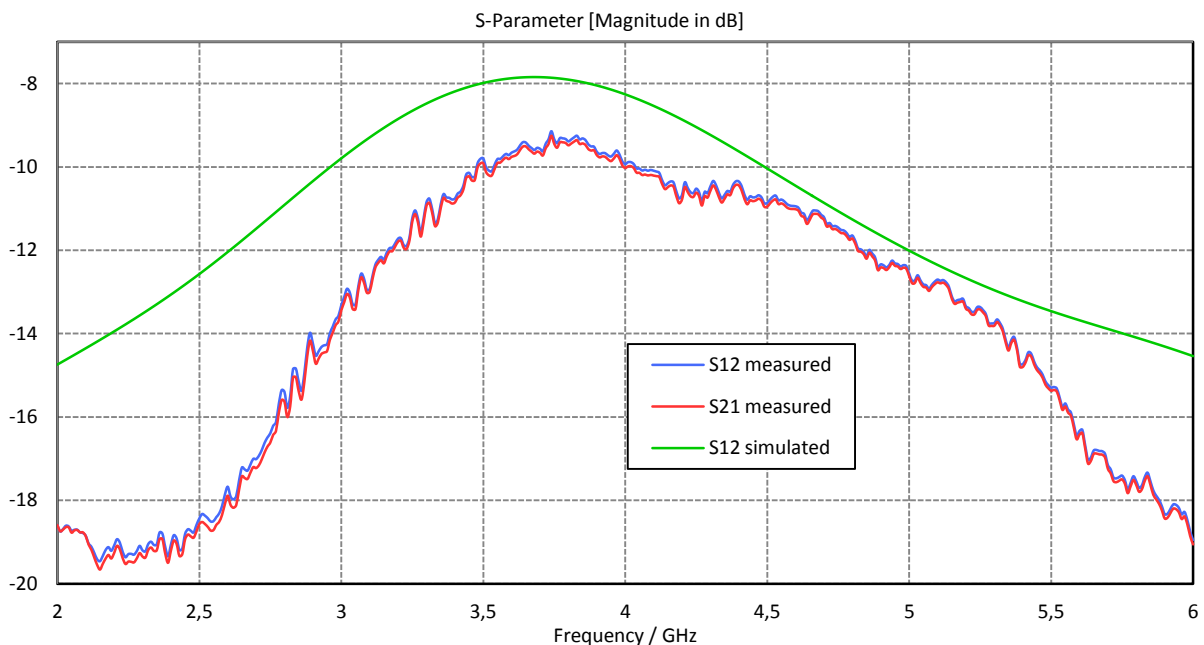


Figure 43:  $S_{12}$  and  $S_{21}$  measured and simulated

Within the operating bandwidth, the coupling factor (Figure 43) between the two antennas is less than -9 dB and therefore better than in the simulations.

### 5.4.5 Antenna pattern

The antenna patterns were measured with a fully automatic setup in the anechoic chamber (Figure 44). The measurement process is controlled by a measurement software from Rohde&Schwarz. The device under test (DUT) is mounted on top of the rotating table (Figure 44, middle). The unbalanced signal is transformed to a balanced signal with the described balun and split with two power splitter for both dipoles. This equipment is hidden in the cylinder. This table is rotating from  $0^\circ$  to  $360^\circ$  and represents the angle  $\phi$  as in the simulations. The measurement antenna (Figure 44 top: black horn antenna) rotates from  $0^\circ$  to  $160^\circ$  and represents  $\theta$ . The missing  $20^\circ$  cannot be physically measured because of the presence of the rotating table.

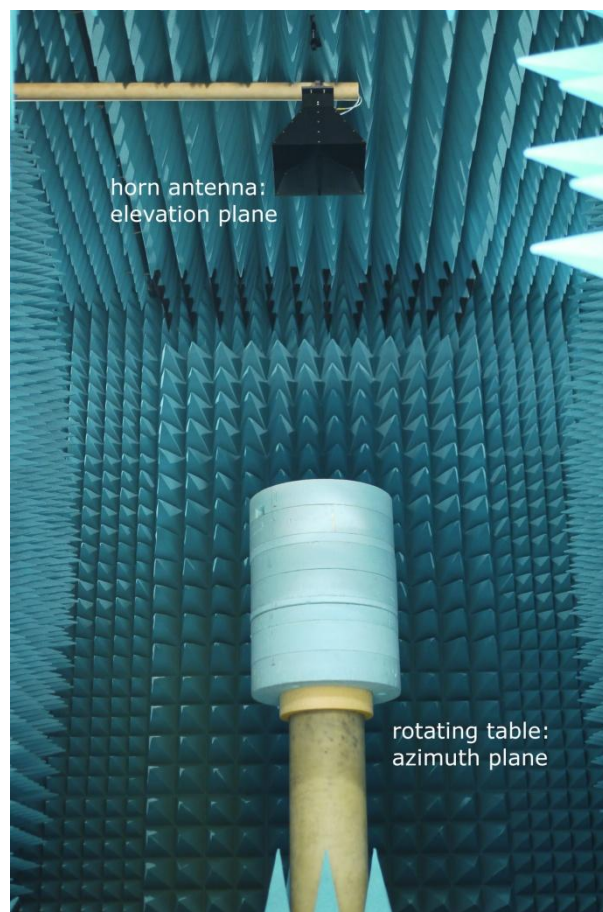


Figure 44: Measurement chamber

The measurement itself is done with the ZVA24 again. The vector analyzer measures  $S_{12}$  between the DUT (ZVA24 Port 1) and the measurement antenna (ZVA24 Port 2) at far-field distance. The measurements were done with a step size of  $5^\circ$  for the angle and 10 MHz for the measurement frequency. The start frequency was set with 3 GHz. In comparison to the

simulations the start frequency was different, caused by the calibration of the chamber. The stop frequency was set at 6 GHz as for the simulations. According to the required bandwidth (3.5 GHz – 4.5 GHz) the measurement below 3 GHz can be neglected.

In the following plots, the antenna pattern for different frequencies of the double dipole antenna is shown. The measurements are plotted in the same way as the simulation for an easy comparison.

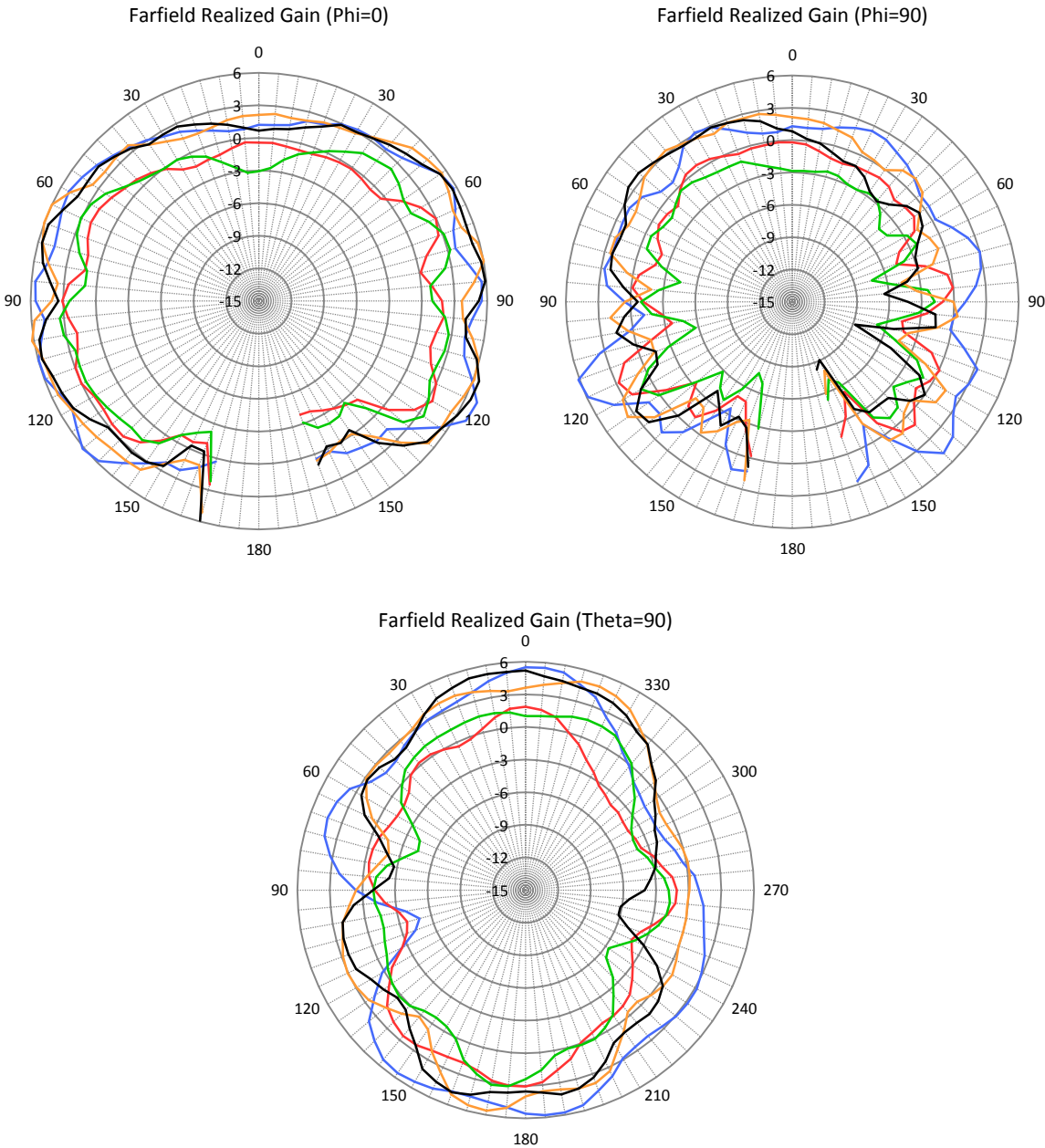


Figure 45: Far-field plot for different frequencies:

3.5 GHz (blue), 3.75 GHz (red), 4 GHz (green), 4.25 GHz (orange), 4.5 GHz (black)

Figure 45 shows the far-field plot for different frequencies within the required bandwidth. The pattern shows the omnidirectional behavior of the antenna for all frequencies.

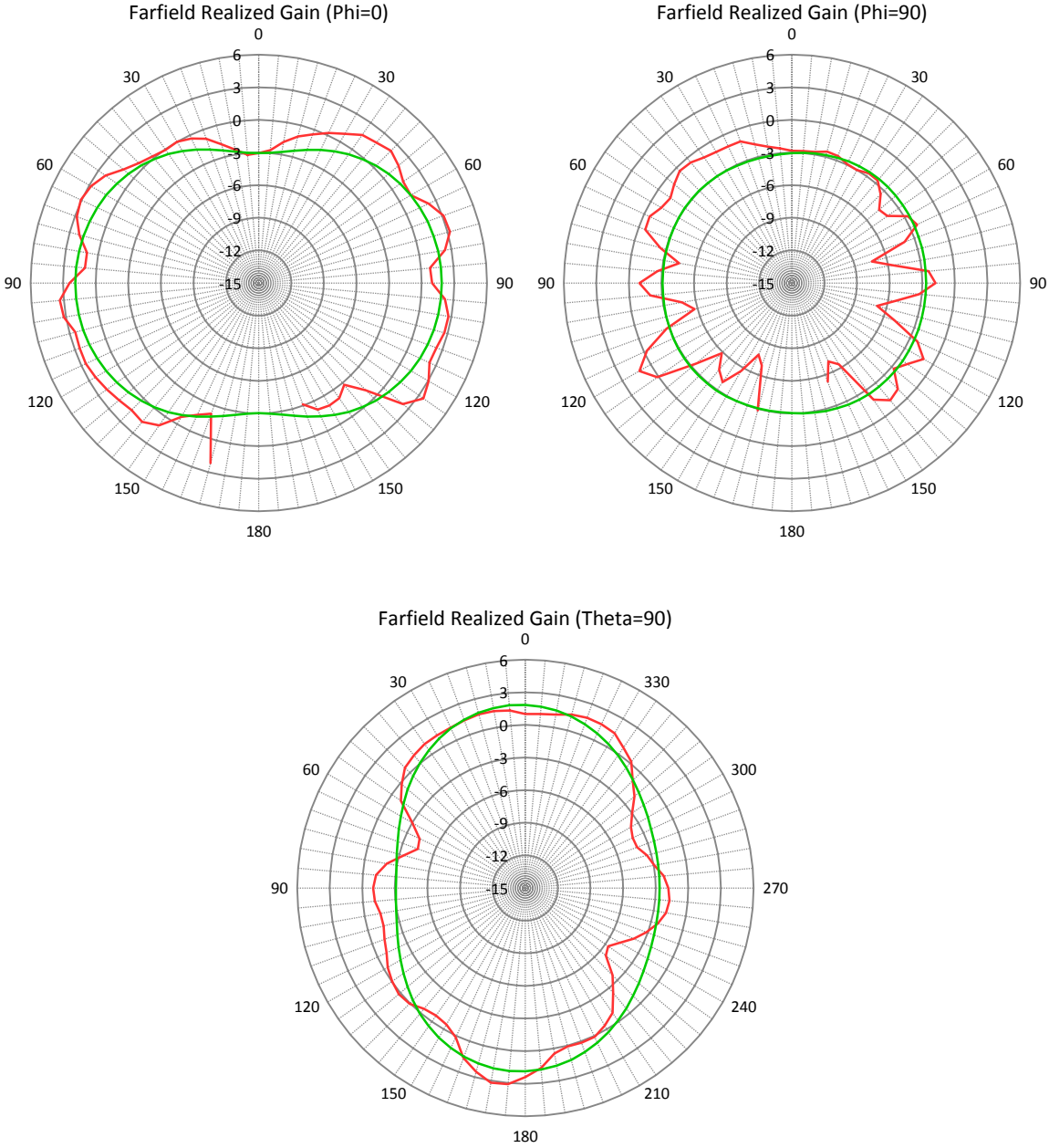


Figure 46: Far-field plot comparison of measured and simulated at 4 GHz:  
measured pattern (red), simulated pattern (green)

The comparison between the simulation and the measurement at 4 GHz is shown in Figure 46. Apart from a slight variation of the gain (explained below), the measured pattern matches well with the simulation.

The connection by metal semi-rigid cables (Figure 47) and other metal parts (balun and power splitter) close to the antenna causes reflection and shielding effects in the pattern. Especially in Figure 46 (upper right plot: Theta, Phi=90), for an angle below 90° the effect of the cables are evident. These effects can be hardly eliminated for those measurements.

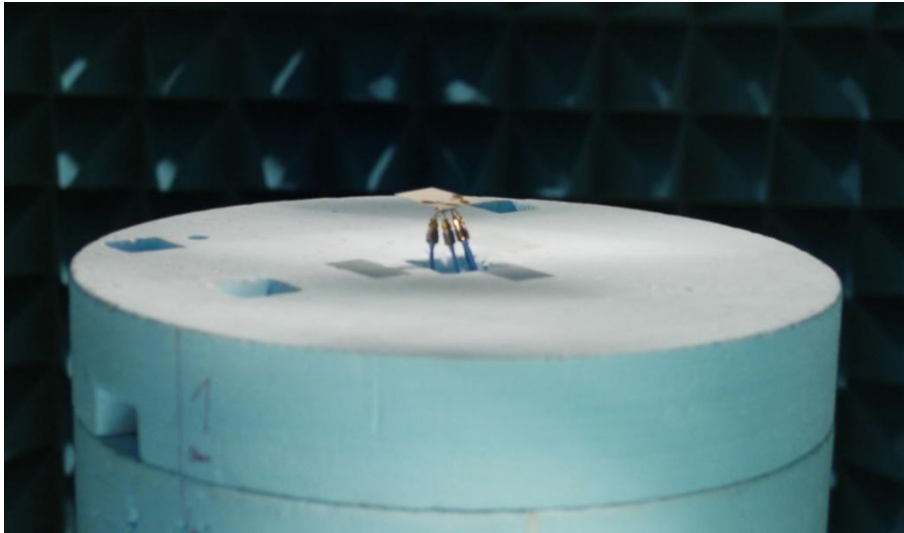


Figure 47: Connected antenna in the chamber

Caused by the used feeding equipment (balun and power splitters) every single radiator (Dipole 1  $\pm$  and Dipole 2  $\pm$ ) is fed with a slightly different magnitude and phase. The balun causes a phase shift of  $\pm 2^\circ$  between the two outputs. The measurement antenna captures all radiated waves of the antennas and adds them together to one electric field in one point in space. Because of the different signals at the feed of the DUT and with it the different radiated waves in amplitude and phase, the gain varies with the direction and the frequency. This explains the ripple of the patterns and the large variation of the antenna gain (Figure 48). The shown far-field patterns are the result of  $S_{12}$  measurements between the input of the balun (end of the calibrated chamber cable) and the output of the measurement horn antenna. Therefore, only the attenuation of the balun and the power splitters can be considered in total, but not the phase shifts between one to another radiator.

#### 5.4.6 Antenna gain

Out of the measurements for the polar radiation plots, the antenna gain (Figure 48) over the frequency has been also evaluated. In this figure the effects of the feeding construct on the pattern at different frequencies are apparent. The metal structure under the antenna PCB causes an average increase of 3 dB for the gain in the z-direction (Theta=0, Phi=90).

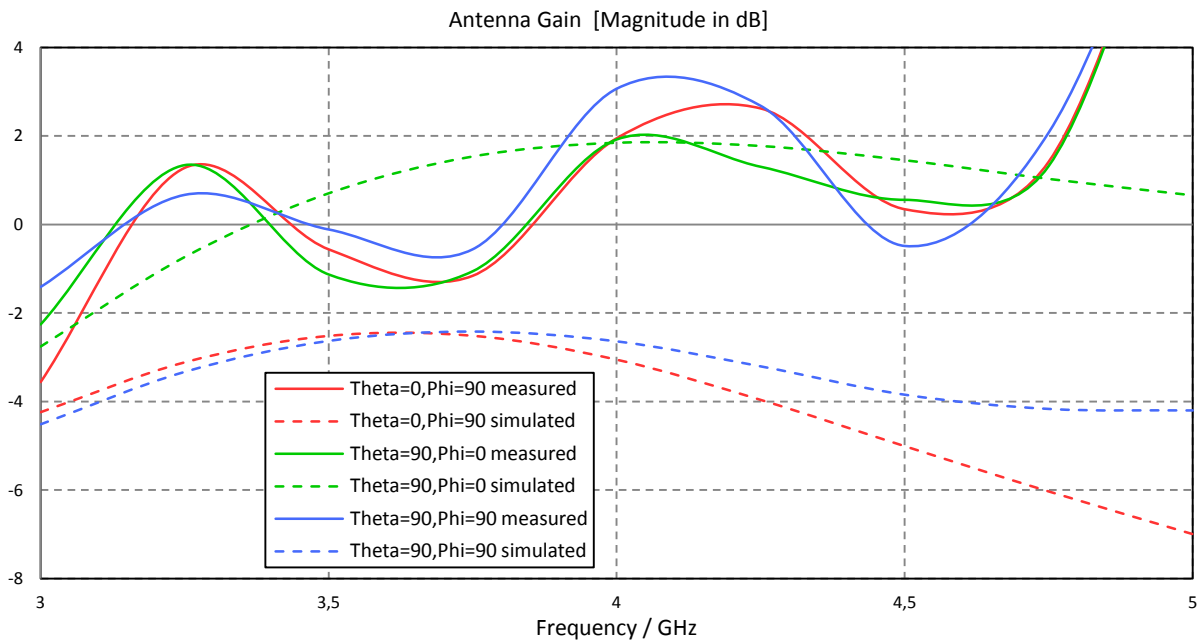


Figure 48: Antenna gain

Also the phase shift effects, as mentioned before, vary with the frequency and cause the large ripple of the gain over the used bandwidth. Taking these effects into account, the shape of the measured antenna gain is comparable with the simulations.

#### 5.4.7 Group delay

The group delay was measured in the balanced mode of the ZVA24 in the anechoic chamber. The analyzer was placed in the middle of the chamber and shielded with some absorbers. Two antenna PCBs were placed in a distance of 30 cm facing each other (Figure 49).

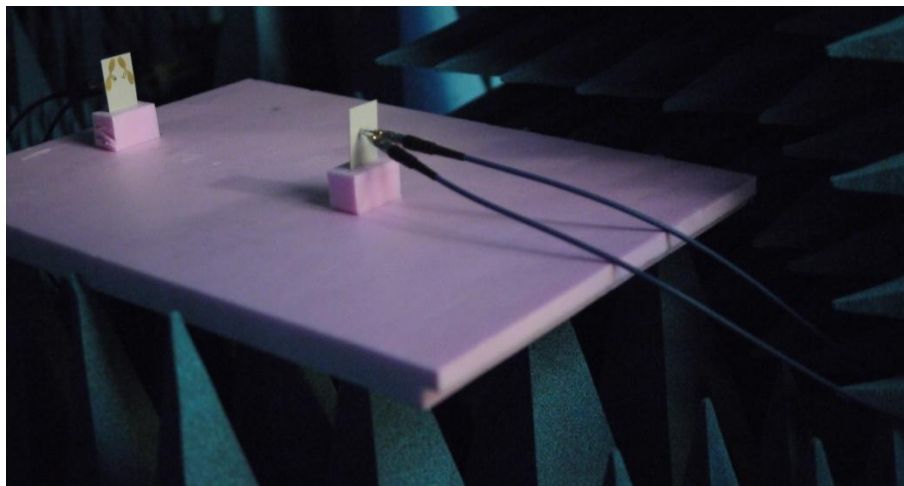


Figure 49: Measurement setup group delay

One antenna on each PCB was matched with  $100 \Omega$  and the other one was used for the measurement. The network analyzer had to be placed in the chamber, because two pairs of similar and long enough cables and the connectors into the chamber were not available.

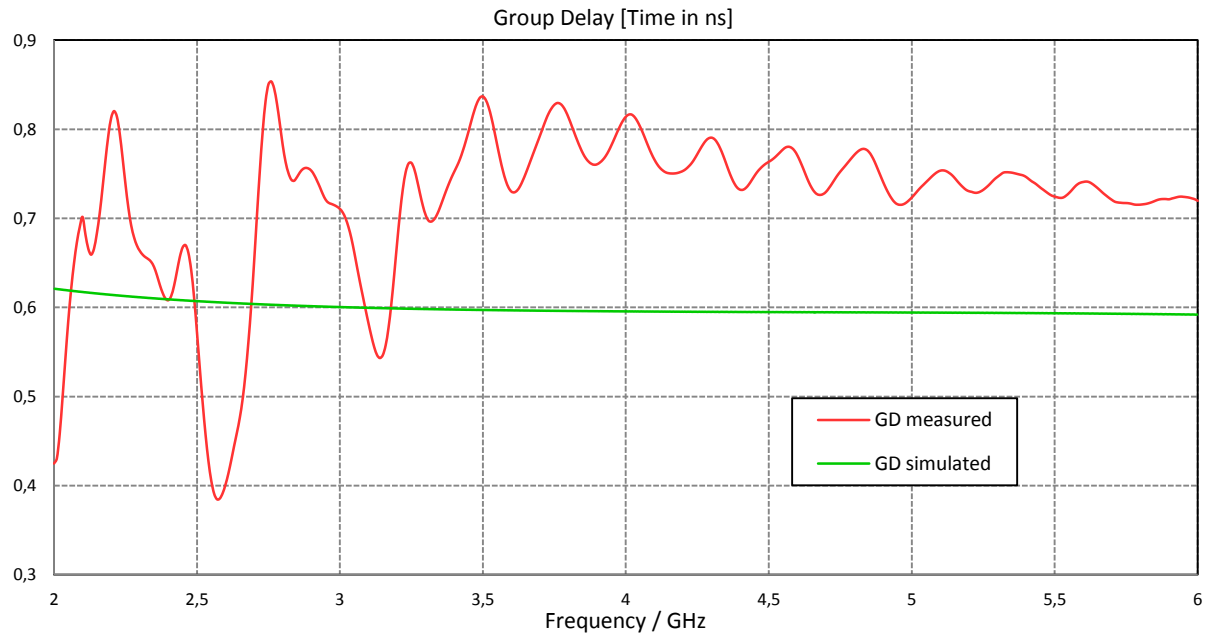


Figure 50: Group delay measured and simulated

Figure 50 shows the measured and the simulated group delay. The variation between of the curve within the used bandwidth is the significant value. As shown in the simulations before (Figure 36) the variation is 0.01 ns. In comparison to the measured values,  $\tau_g$  increase to 0.1 ns. The large variation below 3.5 GHz is caused by the miss-match of the antenna at these frequencies and it can be neglected for our purposes.

## 6 Planar Inverted-F Antennas

Inspired by the small package size like in paper [27], PIFAs could be a good alternative to the dipole antennas. Even though in Paragraph 4.3.2 PIFAs are mentioned as less suitable due to the ground plane and a large number of antennas needed to omnidirectionally cover the whole pattern, simulations were performed in order to study this structure.

### 6.1 Stages of development

Starting from a standard design, as shown in Figure 19, in consideration of miniaturization techniques, a planar inverted-F antenna was designed.

#### 6.1.1 Radiator

The radiator values ( $rad_x$ ,  $rad_y$ ,  $rad_z$ ) and also the length of the shortcut plane determine the used center frequency of 4 GHz. The height of the antenna should be as small as possible. The ratio of length to width should be around 2:1 to achieve a good utilization of space. By adapting the Equation 4.2 with given values, it is possible to obtain the Equation 6.1.

$$\frac{\lambda}{4} \approx \sqrt{\frac{\epsilon_r + 1}{2}} (rad_z + rad_x + rad_y - feed_y_2) \quad 6.1$$

With respect to the used substrate with the given  $\epsilon_r$  the geometrical parameters of the radiator were estimated. During the simulations the variables were tuned to achieve optimal results (see Table 6).

#### 6.1.2 Substrate

To show the effects of the added substrate and its permittivity the first design was simulated with vacuum in between the GND plane and the radiator. By adding different substrates, the size could be reduced and the performance improved.

### 6.1.3 Feeding structure

The biggest challenge was to design the PIFA for the given broadband specifications. This could be achieved by changing the feeding structure. The first step was to simulate different feed shapes. Common PIFAs use a flat metal plate on one side of the cube. For this antenna, the best feeding configuration could be achieved with a round via.

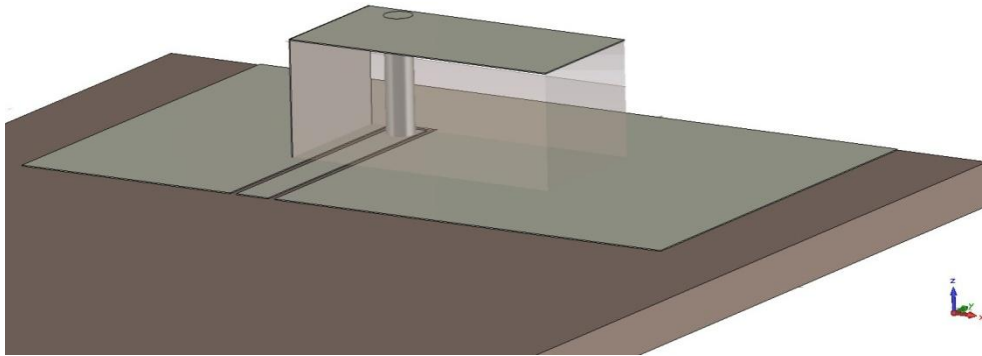


Figure 51: PIFA design

The next step is to find the best position of the feed. In this case two degrees of freedom can be set ( $x$ - and  $y$ -direction). The via-hole is placed inside the cube but as far from the backside of the substrate cube as possible. The feed itself is designed for an input impedance of  $50 \Omega$ . To set this impedance the width of the feed ( $feed\_x\_1$ ) and the gap ( $a$ ) to the ground plane are used. The distance to the ground feed ( $d$ ) and with it the  $y$ -direction of the feed are also important for the matching.

### 6.1.4 Ground plane

Depending on the influence of the ground plane to the other sub-systems on the key, the used space has to be minimized. Therefore, a specific step of this development was used to investigate the smallest possible ground plane.

With these adaptations, the single antenna (Figure 51) fulfills the specifications. In the next stage, several PIFAs should be placed by the given PCB to obtain an omnidirectional pattern.

## 6.2 Simulations

The settings for CST Microwave Studio and a short description for the measurements are mentioned in Chapter 2 and 3. In this part, only the results are shown and discussed.

### 6.2.1 Parameters

In CST all variables of the different shapes are parameterized. The used variables of the antenna (Figure 52) and the final values are shown in Table 6.

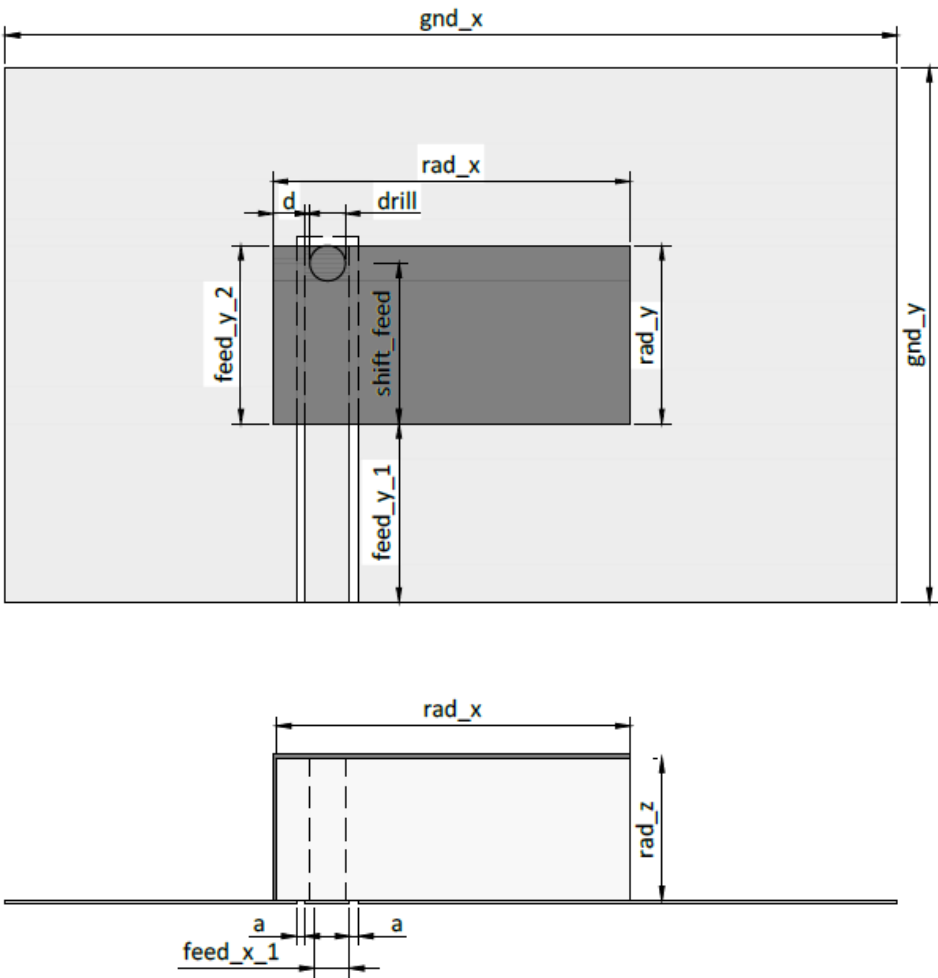


Figure 52: PIFA parameters

Variable		Value		Description
		flat	round	
<i>a</i>	mm	0.25	0.25	Distance between feed and ground plane
<i>d</i>	mm	3.75	0.9	Distance between feed and ground feed
<i>rad_x</i>	mm	16	10	Length of the radiator
<i>rad_y</i>	mm	6	5	Width of the radiator
<i>rad_z</i>	mm	5	4	Height of the radiator
<i>drill</i>	mm	-	1	Diameter of the via
<i>feed_x_1</i>	mm	1.25	1.25	Feed 1 width
<i>feed_y_1</i>	mm	5	5	Feed 1 length
<i>feed_y_2</i>	mm	6	5	Feed 2 width
<i>shift_feed</i>	mm	-	4.5	Shift of feed in y-direction
<i>shift_x</i>	mm	0	0	Antenna shift out of x=0 position
<i>shift_y</i>	mm	40	42	Antenna shift out of y=0 position
<i>gnd_x</i>	mm	32	25	Length of the GND plane
<i>gnd_y</i>	mm	15	15	Width of the GND plane
<i>metal_h</i>	mm	0.035	0.035	Metal height
<i>sub_x</i>	mm	32	32	Dimensions of the PCB substrate
<i>sub_y</i>	mm	52	52	
<i>sub_h</i>	mm	1.5	1.5	

Table 6: PIFA parameters

The focus of these simulations was to prove the feasibility of PIFAs for this application. Therefore no simulations for side effects are reported and only the PIFA properties itself are shown.

## 6.2.2 Reflection coefficient $S_{11}$

In the following 2 figures  $S_{11}$  is shown for a design with a flat feed (Figure 53) and for a round feed (Figure 54). For both designs, different materials for the substrate of the cube have been investigated.

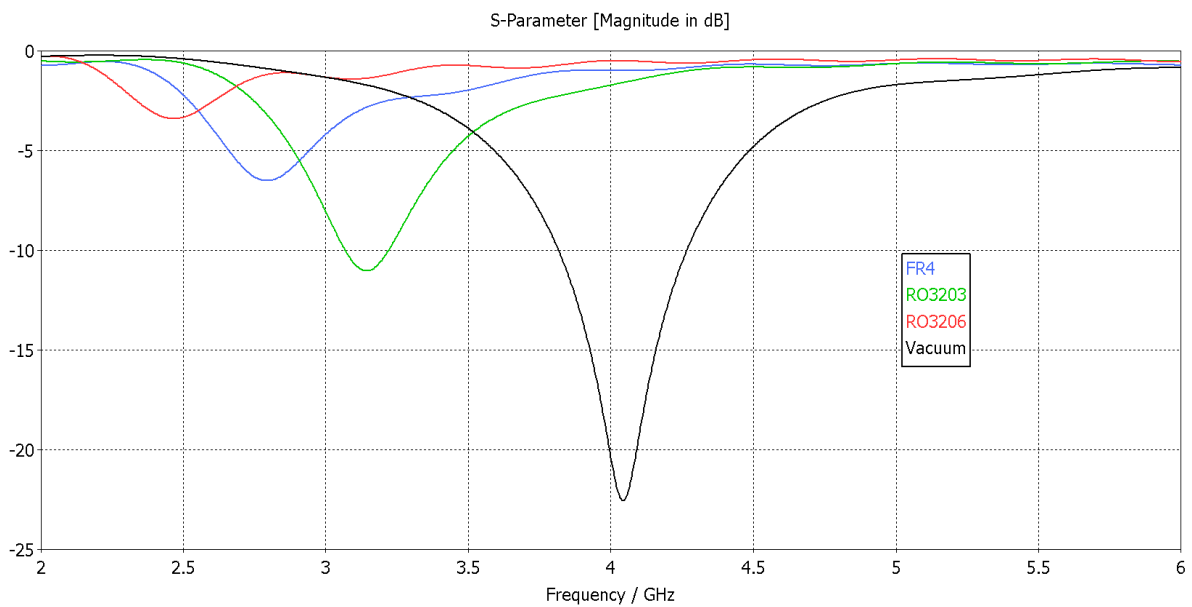


Figure 53:  $S_{11}$  comparison for flat feed with different substrate

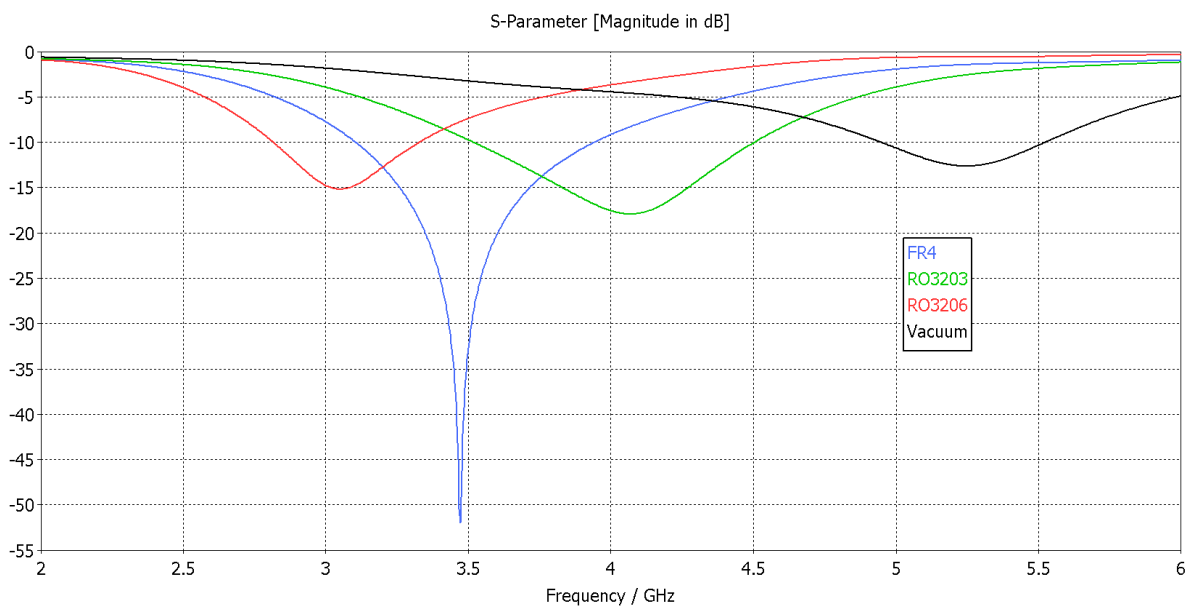


Figure 54:  $S_{11}$  comparison for round feed with different substrate

In Figure 53, the simulations are based on an antenna dimensioned for vacuum (black curve). By using a substrate with a given permittivity the resonant frequency of the antenna decreases.

The next analysis/design step is shown in Figure 54. The flat feed was replaced by a round feed and the antenna was designed for a permittivity  $\epsilon_r = 3$ . In comparison to other substrates, RO3203 provides the best ratio of bandwidth, reflection coefficient and size of the antenna.

On the basis of the previous two simulations, all further simulations were carried out with a round feeding structure.

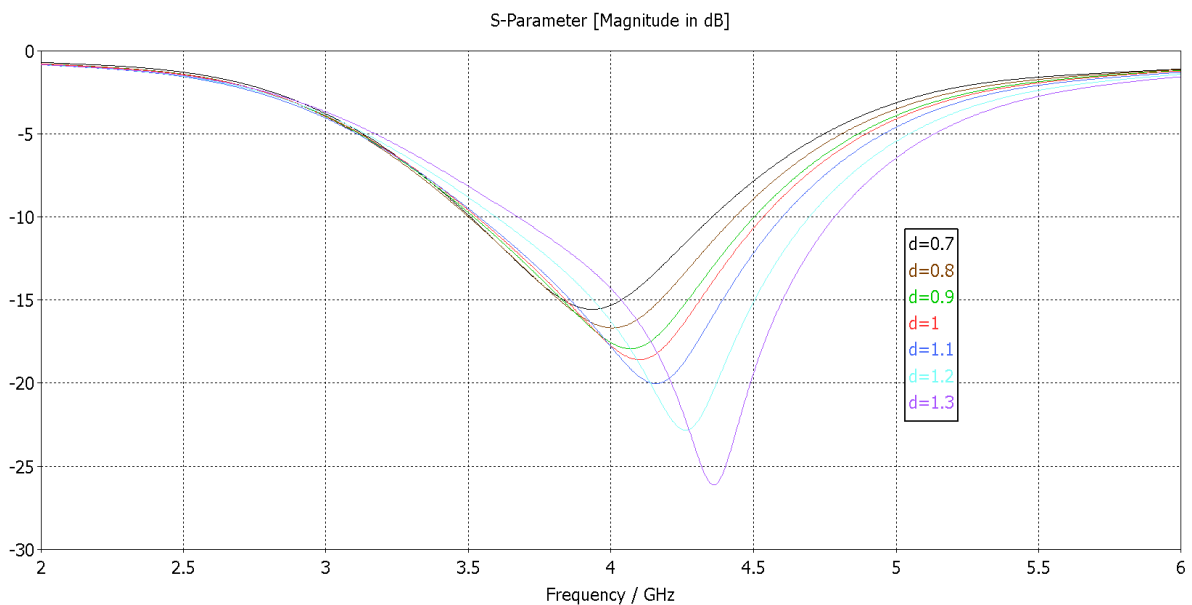


Figure 55:  $S_{11}$  comparison for round feed with different  $d$

Based on the geometry of a PIFA, a number of degrees of freedom are available to adjust the antenna behavior to the given requirements. The position of the feed can be tuned to achieve the best impedance matching and to vary the bandwidth.

In Figure 55, a parameter sweep for  $d$  and in Figure 56 a sweep for  $shift\_feed$  is shown. In both figures, the green curve shows the best result for matching and bandwidth.

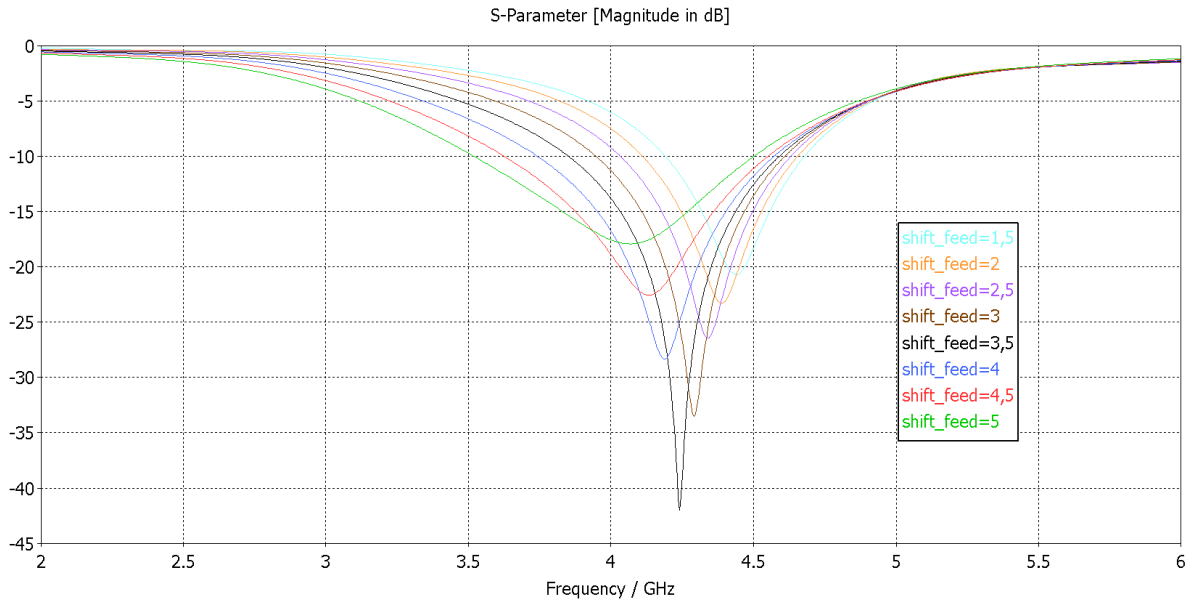


Figure 56:  $S_{11}$  comparison for round feed with different *shift\_feed*

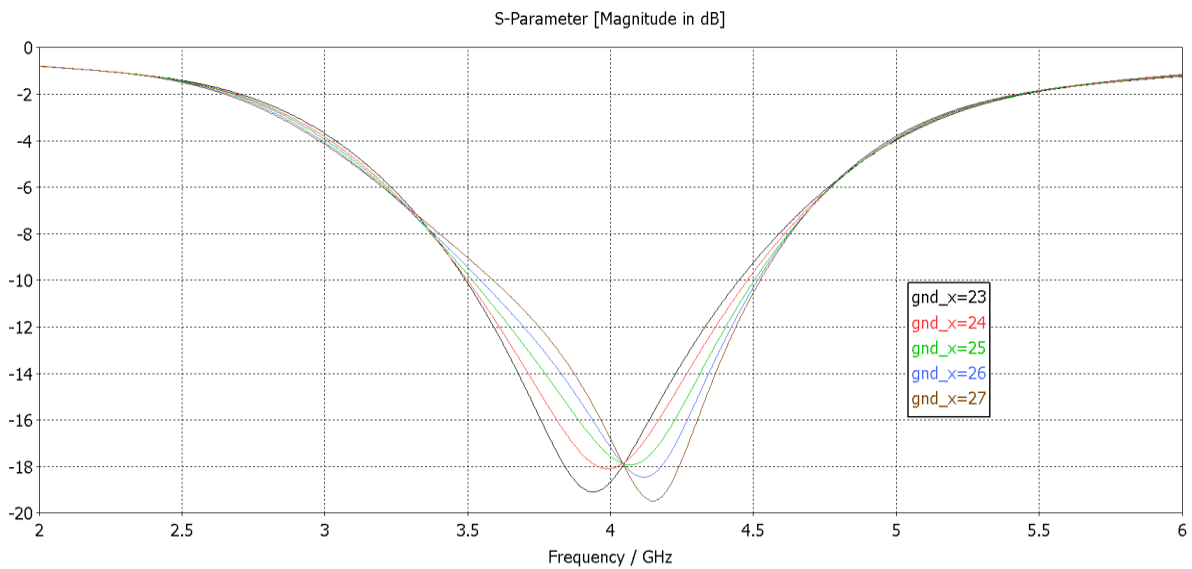


Figure 57:  $S_{11}$  comparison for round feed with different *gnd\_x*

One of the biggest effects on the bandwidth of the PIFA is caused by the ground plane. For this special application, the ground plane is the crux. As mentioned before, the designed ground plane should be as small as possible. A certain minimal size is anyway required for a reasonable behavior of the antenna.

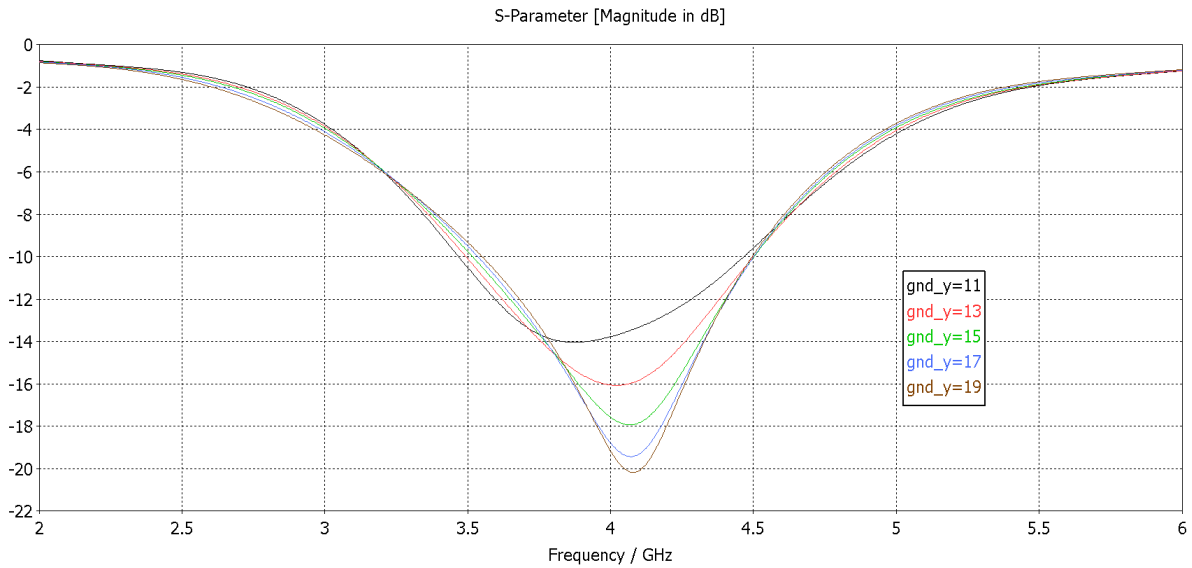


Figure 58:  $S_{11}$  comparison for round feed with different  $gnd\_y$

In Figure 57 and Figure 58, an outline of different sizes of  $gnd\_x$  and  $gnd\_y$  around the best case (green line) is shown. The result of this simulation run was a ground plane with a size of  $gnd\_x=25$  and  $gnd\_y=15$ . Specially by decreasing  $gnd\_x$ , the bandwidth breaks decrease too (Figure 57).

In comparison to the size of the whole PCB with a width of 32 and a length of 52, the GND-plane of a single antenna is already using a huge part of the board.

### 6.2.3 Antenna pattern

The simulations for the antenna pattern of a PIFA were only done for the final antenna version with the round feed (Figure 52 and Table 6).

The impact of the ground plane on the radiation pattern is evident. In negative z-direction (Figure 59 - left plot) the gain is significantly attenuated. In the azimuth plane (Figure 59 - right plot) two minima are present.

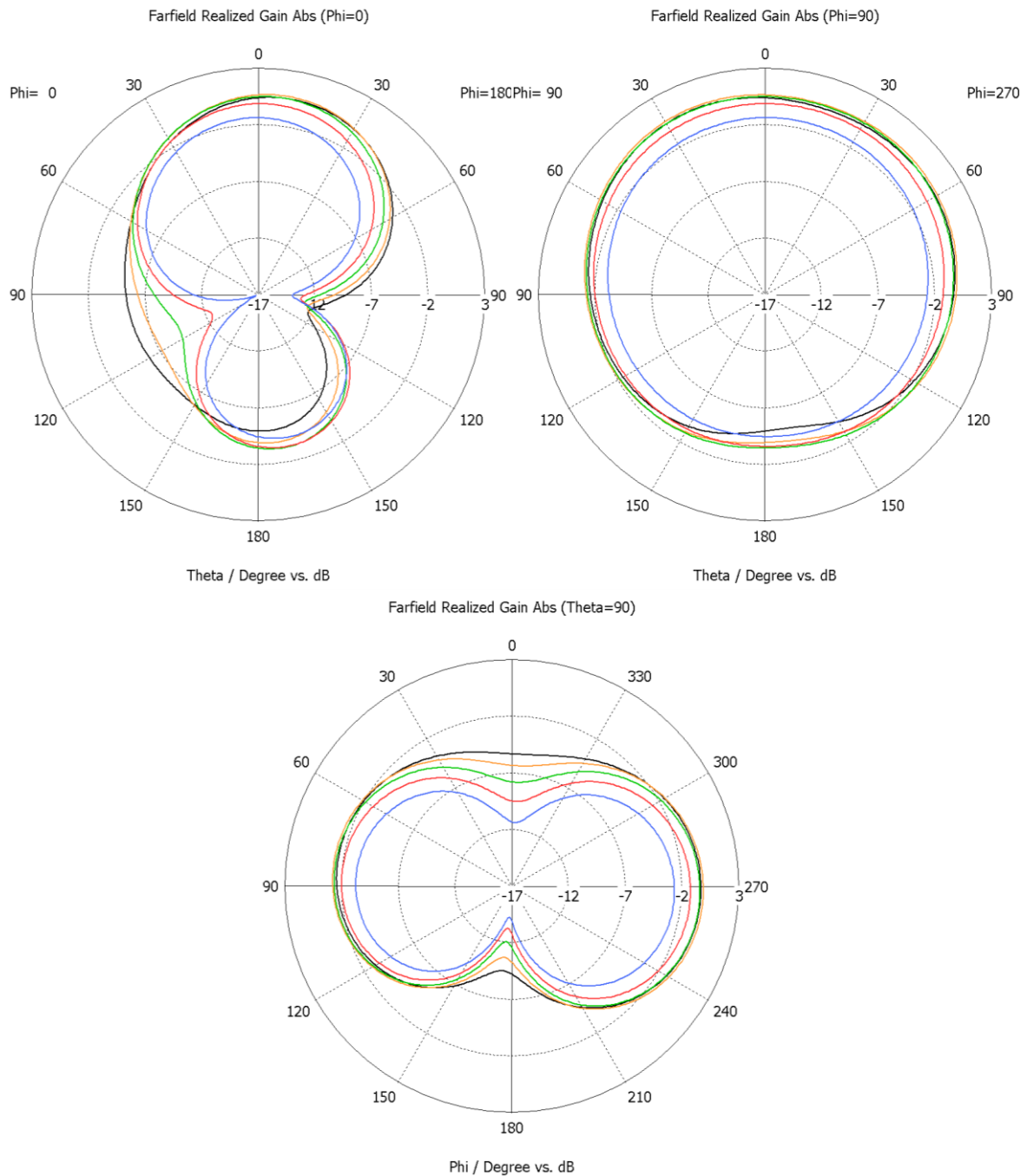


Figure 59: Far-field plot with PIFA for different frequencies:

3.5 GHz (blue), 3.75 GHz (red), 4 GHz (green), 4.25 GHz (orange), 4.5 GHz (black)

The main finding from this first pattern is that an omnidirectional characteristic is hardly realizable with planar inverted-F antennas. The minimum in the negative z-direction can be avoided by adding a second PIFA on the bottom side of the PCB. For the given specifications and space limitations of the key-application, this is unfortunately not possible. Even if the PIFA height would be reduced to fit in the key, the minima in the azimuth plane would still

appear. This problem could be only hypothetically fixed by adding two additional 90°-titled antennas to the PCB. Because of the ground plane, this is practically not possible.

Another problem of the miniaturized PIFAs is the difficult manufacturing process. A thick ceramic cube with a required permittivity, two metalized surfaces and a drill through a hard material are require a complex and expensive manufacturing process.

This investigation shows that the planar inverted-F antenna is not usable for the final application. Therefore final prototypes were not designed nor manufactured.

## 7 Conclusions

In this thesis a UWB dual-polarized antenna system for a handheld automotive application has been developed. Several designs were investigated, such as dipole-, monopole- and planar inverted-F antennas. Dipoles were chosen as the best-fitting design for the given requirements and they were used as the basic antenna structure for the whole work. In comparison to other designs, dipoles offer advantages like absence of a ground plane (reduced space occupation), broadband behavior with special designs and, through a combination of two dipole antennas, a quasi-omnidirectional pattern can be achieved. A special structure with two broadband dipole antennas was designed to reach the desired performances. The biggest issue was to minimize the antennas inside the given size available on the key by keeping the desired RF-performances.

### 7.1 Results

The antenna was designed and tested through several steps: simulation and optimization, manufacturing and measurements. The final simulation and measurement results are listed in Table 7.

Characteristic		Simulation	Measurement
$f_c$	GHz	3.9	3.9, 4.1
Dimensions	mm <sup>2</sup>	52 x 32	
$\epsilon_r$		6.15	
$\tan \delta$		0.0027	
BW	GHz	1	1.5
max $G_o$ @ 4 GHz	dB	1.8	3
variation of $\tau_g$	ns	0.01	0.1

Table 7: Final results

The required specifications are fulfilled. The bandwidth is larger than 500 MHz, a quasi-omnidirectional antenna pattern is given and caused by a high dielectric constant of the

substrate the antenna size for a center frequency of 4 GHz could be reduced. The coupling was reduced to a minimum and the estimated group delay variation is negligible.

With the simulations the limits of the antenna and of the miniaturization techniques were investigated. The dipole design offers a good compromise of size, RF-specifications, and an economic production. Within the simulated limits, a prototype was manufactured. The simulated performances were verified through measurements. Taking the side effects of the measurements and the equipment into account, the manufactured antenna design matches quite well the simulation results.

## **7.2 Future Work**

This antenna is the handheld RF-part of an automotive system. The next step will be to investigate the interaction of this part with the car antenna and to build up a communication demonstrator. Next to this step, the electronic subsystem for the handheld antenna (e.g. integrated chip, LF-part, battery integration) has to be developed. Finally, a fully functional communication between the key and the car should be provided.

## Bibliography

- [1] FCC, "First Report and Order 02-48," Federal Communications Commission, Washington, D.C., 2002.
- [2] J. Liang, "Antenna Study and Design for Ultra Wideband Communication Applications," Queen Mary, University of London, United Kingdom, 2006.
- [3] C. A. Balanis, *Antenna Theory, Analysis and Design*, third ed., Hoboken, New Jersey: John Wiley & Sons, 2005.
- [4] W. Wiesbeck, G. Adamiuk and C. Sturm, "Basic properties and design principles of UWB antennas," IEEE, 2009.
- [5] "CST," Computer Simulation Technology AG, 2013. [Online]. Available: [www.cst.com](http://www.cst.com).
- [6] "IEEE Xplore," [Online]. Available: <http://ieeexplore.ieee.org>. [Accessed 2012].
- [7] P. Cerný and M. Mazánek, "Optimized Ultra Wideband Dipole Antenna," Czech Technical University in Prague, Prague, 2006.
- [8] H. G. Schantz, *The Art and Science of Ultrawideband Antennas*, New York: Artech House, 2005.
- [9] L. Guofeng, S. Predrag and G. Larry, "Antenna and Pulse Designs for Meeting UWB Spectrum Density Requirements," 2003 IEEE Conference Ultra Wideband Systems and Technologies, 2003.
- [10] H. G. Schantz, "Planar Elliptical Element Ultra-Wideband Dipole Antennas," IEEE - Antennas and Propagation Society International Symposium, 2002.
- [11] G. Quintero and A. K. Skrivervik, "Analysis of Planar UWB Elliptical Dipoles fed by a Coplanar Stripline," IEEE - INTERNATIONAL CONFERENCE ON ULTRA-WIDEBAND, Vol. 1, Lausanne, 2008.
- [12] X. H. Wu and Z. N. Chen, "Comparison of Planar Dipoles in UWB Applications," IEEE TRANSACTIONS ON ANTENNAS AND PROPAGATION, VOL. 53, NO. 6, 2005.
- [13] X. H. Jin, X. D. Huang, C. H. Cheng and L. Zhu, "Super-Wideband Printed Asymmetrical Dipole Antenna," Progress In Electromagnetics Research Letters, Vol. 27, 2011.

- [14] K. P. Ray, "Design Aspects of Printed Monopole Antennas for Ultra-Wide Band Applications," Hindawi Publishing Corporation, International Journal of Antennas and Propagation, Vol. 2008, 2008.
- [15] P. Cao, Y. Huang, J. Zhang and Y. Lu, "A Comparison of Planar Monopole Antennas for UWB Applications," Antennas & Propagation Conference, Loughborough, 2011.
- [16] F. Koshiji, T. Eguchi, K. Sato and K. Koshiji, "Proposal and investigation of a flat type small volcano smoke antenna," International Symposium on Antennas and Propagation— ISAP, 2006.
- [17] Z. N. Chen, "Miniaturization of Ultra-wideband Antennas," Proceedings of the Asia-Pacific Microwave Conference, Australia, 2011.
- [18] Y. Lu, Y. Huang, Y. C. Shen and H. T. Chattha, "A Further Study of Planar UWB Monopole Antennas," Antennas & Propagation Conference, Loughborough, 2009.
- [19] R. Pillalamarri and S. B. Rao, "Analysis on size miniaturization in printed circular disc monopole antennas for UWB communications," IEEE - International Conference on Ultra Modern Telecommunications & Workshops, 2009.
- [20] A. M. Abbosh and M. E. Bialkowski, "Design of Ultrawideband Planar Monopole Antennas of Circular and Elliptical Shape," IEEE Transactions on Antennas and Propagation, Vol. 56, No. 1, 2008.
- [21] F. Yu and C. Wang, "A CPW-Fed Novel Planar Ultra-Wideband Antenna with a Band-Notch Characteristic," RADIOENGINEERING, VOL. 18, NO. 4,, 2009.
- [22] M. Sun and Y. P. Zhang, "Miniaturization of Planar Monopole Antennas for Ultrawide-Band Applications," Antenna Technology: Small and Smart Antennas Metamaterials and Applications, 2007.
- [23] A. K. Skrivervik, J. -F. Zürcher and J. R. Mosig, PCS Antenna Design: The Challenge of Miniaturization, IEEE Antennas and Propagation Magazine, Vol. 43, No. 4, 2001.
- [24] J.-Y. Wen, M.-H. Hsu and J.-F. Huang, "Design of Broadband Planar Inverted F Antenna Using the Resonant Frequency to the next Reactance Equal to Zero," IEEE International Conference on Integration Technology, Shenzhen, 2007.
- [25] Y.-T. Jean-Charles, V. Ungvichian and J. A. Barbosa, "Effects of Substrate Permittivity on Planar Inverted-F Antenna Performances," JOURNAL OF COMPUTERS, VOL. 4, NO. 7, 2009.

- [26] M. C. Hunynh and W. Stutzman, "Ground plane effects on planar inverted-F antenna (PIFA) performance," IEE Proc.-Microw. Antennas Propag., Vol. 150, No. 4, USA, 2003.
- [27] D. Kearney and M. J. Ammann, "Small Ultra-Wideband Antenna for Mobile Handset," Antennas & Propagation Conference, Loughborough , 2009.
- [28] R. Li, G. DeJean, M. M. Tentzeris and J. Laskar, Development and Analysis of a Folded Shorted-Patch Antenna With Reduced Size, IEEE TRANSACTIONS ON ANTENNAS AND PROPAGATION, VOL. 52, NO. 2, 2004.
- [29] "Institute of microwave and photonic engineering," Graz University of Technology, 2013. [Online]. Available: [www.ihf.tugraz.at](http://www.ihf.tugraz.at). [Accessed 2013].
- [30] M. Microwave, "Broadband Balun (200 kHz to 10 GHz) BAL-0010," Marki Microwave, 2012.